Engineering Fracture Mechanics 292 (2023) 109620

Contents lists available at ScienceDirect

Engineering Fracture Mechanics

journal homepage: www.elsevier.com/locate/engfracmech

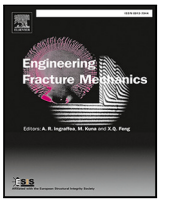

Influence of rate-dependent damage phase-field on the limiting crack-tip velocity in dynamic fracture

Elie Eid *, Anthony Gravouil, Gergely Molnár

Univ Lyon, INSA-Lyon, CNRS UMR5259, LaMCoS, F-69621, France

ARTICLE INFO

Keywords:
Dynamic fracture
Viscoelasticity
Rate-dependency
Crack-branching
Limiting velocities

ABSTRACT

This contribution explores three thermodynamically-consistent damage phase-field formulations for rate-dependent dynamic fracture in viscoelastic materials. By means of a numerical study on a uniform displacement strip benchmark, the formulations and modelling assumptions are compared, and the corresponding limiting crack-tip speeds are discussed. In essence, in addition to recalling the existing phase-field model for viscoelastic materials, a damage phase-field formulation for rate-dependent toughness is introduced as a function of the damage-rate at the crack-tip and is contrasted to existing strain-rate dependent toughness models. Dynamic fracture simulations have demonstrated the significant role of rate dependency in suppressing crack branching and accelerating the crack propagation. The rate dependency is analysed through two main mechanisms: (i) the viscous dissipation, which can promote fracture, and (ii) an increase in the energy required to evolve a crack, through rate-dependent toughness models. Depending on the specific choice of parameters, the numerical simulations show crack propagation at speeds that exceed the theoretical limit depicted by the Rayleigh wave speed. Indeed, these high speeds are attributed to the viscoelastic and viscoelastic-like (observed in the case of strain-rate dependent fracture toughness) stiffening at the crack-tip, which translates to faster running surface waves and enables supersonic crack-speeds; a never-seen-before result in damage phase-field simulations.

1. Introduction

Viscoelastic materials such as polymers, gels, metals and alloys play a vital role in various engineering and practical applications. Their widespread use in fields like biomechanics, materials processing, and structural design makes them highly relevant in modern-day technology and innovation. Of course, understanding how such materials fail and elaborating on how to prevent their failure is particularly important to design safer and more reliable structures.

Viscoelastic materials are commonly recognised for their time-dependent mechanical behaviour. For instance, when a viscoelastic structure is subject to a constant load, the material continues to gradually deform over time (creep or relaxation). As the material deforms, higher stress concentrations can develop in localised areas, which can eventually result in the structure's failure. Of course, the time-dependency of the viscoelastic materials translates to a mechanical behaviour that is also rate-dependent; this implies that their deformation and response to loading vary with the velocity of the loading [1]. So, besides the quasi-static failure of viscoelastic materials, dynamic fracture is particularly of relevant interest, especially in impact and high-speed events. In such cases, inertial effects are prominent, and the rate at which the structure is loaded directly influences the amount of stored energy and the amount

* Corresponding author.
E-mail addresses: elie.eid@insa-lyon.fr (E. Eid), anthony.gravouil@insa-lyon.fr (A. Gravouil), gergely.molnar@insa-lyon.fr (G. Molnár).

https://doi.org/10.1016/j.engfracmech.2023.109620
Received 25 May 2023; Received in revised form 31 August 2023; Accepted 7 September 2023
Available online 21 September 2023

of energy that can be dissipated by the viscous effects, thus modifying its fracture behaviour. Accordingly, modelling of fracture in such rate-dependent materials is of increasing interest.

The inclusion of inertial effects (dynamic fracture) introduces the notion of limiting crack-tip speeds. It is widely known that crack propagation is theoretically limited to the Rayleigh wave speed (c_R), although such speed is hardly achieved in real-life applications and numerical simulations [2–9]. Indeed, cracks were shown to become unstable and branch at 40%–60% of the Rayleigh wave-speed. The experimental works of Corre et al. [10] and Morishita et al. [11] reveal that there are instances where the crack-tip speed exceeds the Rayleigh wave speed under high imposed stretches in polymeric elastomers. Earlier experimental works on the fracture of elastomer membranes [12,13] also report such phenomena, and they attribute those high crack-tip speeds to an increase in the stiffness of the material in the vicinity of the crack tip, either because of viscoelastic effects or the hyperelastic stiffening. Kamasamudram et al. [14] attribute these observations to the viscoelastic stiffening of the material by simulating the experiments found in Corre et al. [10]. However, the analysis was done without explicitly modelling crack-propagation, and the crack speeds were implicitly imposed on the geometry as boundary conditions for the numerical simulations.

Since the 20th century, efforts have been devoted to model rate-dependent fracture in viscoelastic materials. Knauss [15] provides a comprehensive 50-year review on theories developed to understand fracture in viscoelastic materials. Thouless et al. [16], for instance, were among the first to describe a generalisation of linear elastic fracture mechanics to add rate dependence to the fracture process. Schapery et al. [17], were the first to extend the traditional J-integral method used in linear elastic fracture mechanics to account for viscoelastic strains. Besides the theoretical methods [15,17,18], many numerical techniques for simulating crack initiation and propagation have been developed in recent decades. Between others, Zhang et al. [19] investigated viscoelasticity with the extended finite element approach [20], Bažant et al. [21] formulated a time-dependent generalisation of the cohesive crack model [22], and Yoon and Allen [23] developed a cohesive zone model applicable to viscoelastic materials. Further, through the continuum damage mechanics approach [24], rate dependence was introduced to the local and non-local damage models [25,26] to investigate the dynamic crack behaviour.

More recently, the damage phase-field approach to fracture has proven to be a powerful tool for the prediction of crack phenomena. In fact, it has several advantages over traditional fracture mechanics methods, including the ability to capture complex crack patterns, handle crack nucleation and propagation in a unified manner, and account for material heterogeneity and anisotropy. The technique is also well-suited for simulating fracture in three-dimensional complex geometries.

The phase-field model was first introduced for fracture problems by Bourdin et al. [27]. It is based on the variational formulation of Francfort and Marigo [28] of Griffith's theory [29]. And since the introduction of the phase-field model for fracture, it has encountered several developments and implementations. The method was employed to describe elasto-plastic [30–32], thermo-elastic [33]; viscoelastic [34–37], elasto-viscoplastic [38], as well as highly heterogeneous materials [39,40].

Regarding materials with rate-dependent behaviour, the rate dependency can either occur in the bulk, through viscoelastic effects for instance, or at the crack-tip via a rate dependency of the fracture toughness [21]. A first proposal for a phase-field fracture model in viscoelastic solids was put forward by Schänzel [34]. Subsequently, Shen et al. [35] developed a phase-field model for viscoelastic solids by defining the driving force as a combination of the elastic energy and a portion of the dissipated viscous energy, based on experimental findings [1,41,42]. Loew et al. [43] considered a finite linear viscoelastic material model in which the non-equilibrium part of the stored strain energy and the accumulated viscous dissipation are indistinguishable. Dammaßet al. [36] describe a two-way coupling between damage and viscous effects, leading to a unified and thermodynamically-consistent phase-field model for fracture in viscoelastic materials. Besides, motivated by experimental findings regarding the evolution of the fracture toughness with the crack-tip speed [44,45], Miehe et al. [33] studied a strain rate-dependent resistance against fracture and Yin et al. [46] formulated the fracture toughness as a function of the strain rate — a feature that is readily applicable even in a pure elastic body. Various attempts have been made to propose different functions that relate the fracture toughness to the strain rates [33,47,48]. Alternatively, and in the same spirit, we suggest a novel damage-rate dependent toughness formulation.

Apart from the elementary dynamic simulations of crack branching by Hai et al. and Yin et al. in their introductory papers [37, 46], previous works based on the phase-field modelling of fracture have only tackled quasi-static simulations of monotonic loading, creep, relaxation, and cyclic loading, without accounting for inertial effects. By doing so, the potential role of the inertial effects in governing the fracture behaviour is neglected. As mentioned by Molnár et al. [32], in dynamic fracture, the surplus of released energy at the crack-tip can be transformed into kinetic energy. The difference between this additional released energy and the fracture toughness of the material determines how much energy becomes available as kinetic energy. The extra kinetic energy governs the velocity at which the crack propagates and equivalently, it governs the overall fracture behaviour. That being the case, taking into account inertial effects is undoubtedly a crucial step to appropriately analyse rate-dependent and velocity-dependent fracture phenomena from one side, and to thoroughly compare the different modelling assumptions, from the other.

Within this challenging context, this contribution explores three thermodynamically-consistent damage phase-field formulations for rate-dependent fracture in viscoelastic materials. The formulations are applied to analyse dynamic fracture with the inertial effects taken into account. The three rate-dependent formulations are implemented into the Abaqus/Standard UEL phase-field model from Molnár et al. [32]. And by means of a numerical study of dynamic fracture on a uniform displacement strip configuration [5,49–51], the modelling assumptions are compared, and the corresponding limiting crack-tip speeds are discussed.

The paper is organised as follows: A brief overview of the approximation of a crack topology by the phase-field model is given along with the governing equations in Section 2. Subsequently, the three phase-field formulations are exhibited in Sections 2.1, 2.2, and 2.3 for the viscoelastic bulk, strain-rate and damage-rate dependent toughness respectively. Section 3 discusses the rate-dependent fracture simulation, while Section 4 compares the characteristics of the various rate-dependent formulations with regards to the limiting crack-tip speeds. Finally, Section 5 elaborates on the effective stiffening phenomena in rate-dependent materials.

2. Methods

This section portrays the underlying mathematical and physical description of the phase-field approach to model fracture in rate-dependent material. We begin by recalling the basic principles of thermodynamics that will be convenient when formulating the phase-field model for rate-dependent fracture. The classical phase-field formulation of brittle fracture in rate-independent materials and the related energy functional are then presented. Afterwards, the formulation is progressively expanded to incorporate the necessary rate-dependent components.

The thermodynamic principles [52] surrounding the formulation of rate-dependent phase-field models for fracture can be summarised as follows: A thermodynamic system is the ensemble of particles that interact with their surrounding by exchanging mass, heat and mechanical work. Here, we only focus on the closed systems, i.e., a system that does not exchange mass with its surrounding. A reversible process is one that can be exactly retraced along the same path by reversing the changes applied. Elastic deformation is a great example of this reversibility, for if an object undergoes elastic deformation and the applied forces are removed, it returns to its original shape without any permanent changes. Conversely, an irreversible process cannot be reversed by simply reversing the changes applied. A meaningful example of irreversibility is the fracturing phenomenon, where the separation of crack surfaces that usually involves the breaking of atomic or molecular bonds within the material cannot be reversed. Lastly, a dissipative process typically involves loss of energy to the surrounding environment. Viscous dissipation is a pertinent illustration of energy dissipation, as it refers to the conversion of mechanical energy into heat, that is lost (dissipated) into the surrounding.

When it comes to modelling viscoelastic materials, there are two different approaches: single-potential models and double-potential models. These approaches are used to describe the behaviour of viscoelastic materials in different ways. Single-potential models simplify the description of viscoelastic behaviour by using a single potential to represent both the elastic and viscous components; such models are advantageous because they are simpler and computationally less demanding compared to double-potential models. In 1975, Halphen and Nguyen [53] introduced the theory of generalised standard materials (sometimes denoted as standard dissipative materials), the theory suggests that the constitutive behaviour of different types of materials can be derived from a pair of scalar functions that fully characterise their material behaviour. These scalar function are known as thermodynamic potentials: the free energy potential (Ψ) and the dissipation potential (Φ).

The free energy potential, specifically, represents the energy that is stored within the system and that has the ability to produce work. It accounts for both the useable energy that is available to produce work, e.g., elastic strain energy, and the energy that can be converted into other form, while being maintained within the system. On the other hand, the dissipative energy potential refers to the energy that is dissipated or lost from the system. This energy is typically associated with irreversible processes, such as viscous dissipation, a form of energy that cannot be recovered nor reused.

In this paper, the double-potential approach (free and dissipative) will be considered in the developments of the formulations to ensure a thermodynamically-consistent coupling between the phase-field damage and the rate-dependent effects. As we will show, this formulation enables to control the energy transfer between the damage and the mechanical problem, i.e., it enables the control of the quantity of the viscous energy that is assumed to promote fracture [36,41], and the quantity of dissipated (lost) energy (more details about the coupling can be found in Section 2.1).

2.0. Phase-field damage model

The principal idea of the phase-field formulation of fracture is the introduction of a diffuse crack topology. The phase-field method diffuses the sharp crack (Γ) into the volume (Ω) of the solid, circumventing the numerical problems associated with the propagating discontinuity (the crack set).

The theoretical crack-surface (discontinuity) is approximated by a function Γ_{l_c} written in terms of a crack surface density (γ_{l_c}) that is a function of a length scale (l_c) (for the regularisation) and a continuous damage field (d) :

$$\Gamma_{l_c} = \int_{\Omega} \gamma_{l_c}(d, \nabla d) dV \tag{1}$$

The continuous damage phase-field variable describes the material's damage state. In the intact region of the material, d takes the value of 0, while in the smeared crack (of width l_c), $0 < d \leq 1$. Refer to Fig. 1 for a two-dimensional illustration of this notion of regularisation of the crack by the length scale (l_c) through the crack surface density function γ_{l_c}.

Various expressions of the crack-density function γ_{l_c} as a function of the damage phase-field variable d can be found in the literature. In this paper, we adopt the linear formulation (AT1):

$$\gamma_{l_c} = \frac{3}{8 l_c}(d + l_c^2 \nabla d \cdot \nabla d) \tag{2}$$

The adoption of the AT1 formulation guarantees an ideally linear elastic response up to the limiting stress. This is a necessary feature for conducting a thorough analysis of the phase-field model in conjunction with the various rate-dependent components.

The fracture energy can be expressed as a function of the damage variable as:

$$\Psi_f \simeq g_c \gamma_{l_c}(d, \nabla d) \tag{3}$$

where g_c is the critical energy release rate, which corresponds to the amount of energy necessary to open a unit fracture surface. In the following, we will refer to it as the fracture toughness.

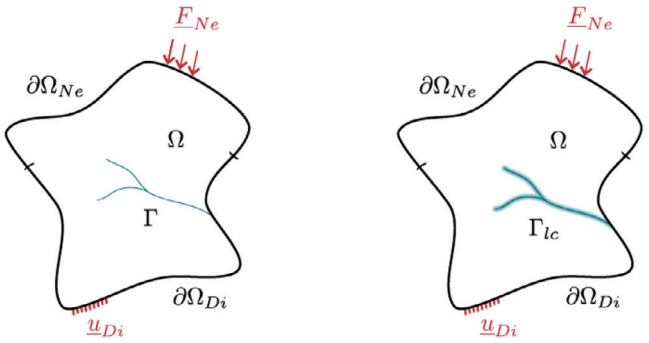

Fig. 1. Regularised representation of a crack in a two-dimensional case, sharp crack (left) and regularised representation through phase-field (right). Ne and Di subscripts stand for Neumann and Dirichlet boundary conditions respectively.

Note that in the case of phase-field modelling of fracture, the fracture energy Ψ_f is not considered a dissipative energy, indeed, it is typically considered as a form of free irreversible energy, in the sense that it is an energy that kept stored in the system within the damage band (irreversible) and not lost to the surroundings.

The regularisation process herein considered results in the need to calculate the elastic strain–energy density (Ψ_e) across the entire deteriorated body. To accomplish this, an energetic degradation function ($g(d)$) is introduced. This function relates mechanical fields (such as strain energy and stress) to the damage phase-field (d), and is inspired by principles from damage mechanics. The specific form of the degradation function used in this study is $g(d) = (1-d)^2$. The elastic strain–energy density Ψ_e becomes a function of the damage-field through the degradation function $g(d)$:

$$\Psi_e(\varepsilon, d) = g(d)\bar{\Psi}_e(\varepsilon) \tag{4}$$

where $\bar{\Psi}_e(\varepsilon)$ represents the 'intact' strain–energy density and ε represents the strain tensor.

Remark 1. Classically, a unilateral contact condition is imposed by splitting the elastic strain energy into a positive part $\bar{\Psi}_e(\varepsilon)^+$ associated to damage and a part $\bar{\Psi}_e(\varepsilon)^-$ which does not activate damage. The strain energy is rewritten as $\Psi_e(\varepsilon, d) = g(d)\bar{\Psi}_e^+(u) + \bar{\Psi}_e^-(\varepsilon)$. The appropriate formulation for the split has been the subject of numerous studies [54,55]. The configuration investigated within this paper is primarily tensile-stress dominant and no crack closure is expected. For that, either the negative part is included or not, the results and conclusions are equivalent. With that in mind, we include the negative part all along and write the elastic strain–energy density following Eq. (4) as: $\Psi_e(\varepsilon, d) = g(d)\bar{\Psi}_e(\varepsilon)$.

The free (stored) energy of a fractured elastic solid is additively decomposed into two parts, the elastic strain energy and the fracture energy:

$$\begin{aligned} \underbrace{\Psi(\varepsilon, d)}_{\text{free (stored)}} &= \underbrace{\Psi_e(\varepsilon, d)}_{\text{reversible}} + \underbrace{\Psi_f(d, \nabla d)}_{\text{irreversible}} \\ &= g(d)\bar{\Psi}_e(\varepsilon) + g_c\gamma_{l_c}(d, \nabla d) \end{aligned} \tag{5}$$

And for the complete elasto-dynamic problem, the energy functional involves the following Lagrangian function :

$$\int_\Omega \mathscr{L}(u, d)d\Omega = \int_\Omega \underbrace{\mathscr{K}(\dot{u})}_{\text{kinetic}} d\Omega - \int_\Omega \underbrace{\Psi(\varepsilon, d)}_{\text{free (stored)}} d\Omega \tag{6}$$

where $\mathscr{K}$ corresponds to the kinetic energy $\mathscr{K}(\dot{u}) = \frac{1}{2}\rho\dot{u}^T\dot{u}$, with ρ the mass density of the material and $\dot{u}$ its velocity, the time derivative $\frac{du}{dt}$ of the displacement u.

For problems where unstable crack propagation is present, the static monolithic solution tends to become numerically unstable [32]. To have a stable implicit formulation, a staggered solution [55] for the phase-field fracture was proposed, so the two subproblems (mechanical and phase-field) can be independently solved:

$$\delta\mathscr{L}(u, d) = 0 \Leftrightarrow \frac{\partial\mathscr{L}}{\partial u}^{0}\delta u + \frac{\partial\mathscr{L}}{\partial d}^{0}\delta d \qquad \forall\delta u, \forall\delta d \tag{7}$$

The notation $\overset{0}{x}$ signifies that x cancels to zero.

This permits taking the variation of both energies to write the corresponding Eulerian equations (strong form) for the displacement problem:

$$\frac{\partial\mathscr{L}}{\partial u} = 0 \quad \forall\delta u \quad \rightarrow \quad \nabla\cdot\sigma - \rho\ddot{u} = 0 \qquad \text{in } \Omega \tag{8a}$$

$$\sigma \cdot n = F_{Ne} \quad \text{on } \partial\Omega_{Ne} \tag{8b}$$

$$u = u_{Di} \quad \text{on } \partial\Omega_{Di} \tag{8c}$$

and for the phase-field problem, where only the free energy (driving force) is typically considered:

$$\frac{\partial \Psi}{\partial d} = 0 \;\; \forall \delta d \rightarrow \quad \frac{\partial g(d)}{\partial d}\bar{\Psi}_e + g_c \frac{\partial \gamma_{l_c}}{\partial d} = -2(1-d)\bar{\Psi}_e + g_c \frac{3}{8l_c}(1 - 2l_c^2 \Delta d) = 0 \text{ in } \Omega \tag{9a}$$

$$\nabla d \cdot n = 0 \quad \text{on } \partial\Omega \tag{9b}$$

$$\dot{d} \geq 0 \quad \text{in } \Omega \tag{9c}$$

while ensuring damage irreversibility by the bound constrained optimisation algorithm [56]. $\ddot{u}$ is the acceleration of the material. σ is the Cauchy stress tensor, n is the unit normal. F_{Ne} corresponds to the forces applied to the boundary $\partial\Omega_{Ne}$, u_{Di} corresponds to the imposed displacements on the boundary $\partial\Omega_{Di}$ (Fig. 1). All implementation details with spatial and temporal discretisation can be found in Ref. [56].

The total mechanical dissipation of an isothermal process, should be non-negative and can be written from the Clausius–Duhem inequality as:

$$\begin{aligned} \dot{D} &= \sigma : \dot{\varepsilon} - \dot{\Psi} \geq 0 \\ &= \sigma : \dot{\varepsilon} - \left(\frac{\partial \Psi}{\partial \varepsilon} : \dot{\varepsilon} + \cancelto{0,\text{ from Equation (9a)}}{\frac{\partial \Psi}{\partial d}\dot{d}} \right) \\ &= \underbrace{\left(\sigma - \frac{\partial \Psi}{\partial \varepsilon}\right)}_{0} : \dot{\varepsilon} \geq 0 \end{aligned} \tag{10}$$

The 'over-dot' $\dot{()}$ denotes the time derivative $\frac{d}{dt}$. Although the damage is irreversible, in the context of the phase-field problem, intrinsic mechanical dissipation is absent; as the material is damaged, the energy is stored in the system as a fracture (surface) energy and not dissipated into its surroundings.

From Eq. (10), the Cauchy stress is written as:

$$\sigma = \frac{\partial \Psi}{\partial \varepsilon} = \frac{\partial \Psi_e}{\partial \varepsilon} + \cancelto{0}{\frac{\partial \Psi_f}{\partial \varepsilon}} = g(d)\frac{\partial \bar{\Psi}_e}{\partial \varepsilon} \tag{11}$$

After showcasing the classical rate-independent phase-field model of fracture, rate-dependent ingredients are added to the problem towards a thorough rate-dependent damage phase-field formulation. It is considered that the rate dependency in a damaging material can either occur in the bulk, through viscoelastic effects for instance, or at the crack-tip via a rate dependency of the fracture toughness.

For each subsequent model, the total free energy, the internal energy production, the updated expression of the stresses, the strong form of the phase-field problem and the thermodynamic consistency of the model are progressively detailed.

2.1. Viscoelasticity

In case of viscoelastic materials, the energy dissipation mechanism at the vicinity of a crack has two main contributions [35]: the processes advancing the crack in the fracture process zone (the innermost closest region to the crack tip), and the viscous dissipation in the bulk. The viscous dissipation in the bulk stems from the irreversible processes in the viscous material and refer to the actual loss of energy. It usually manifests by a generation of heat. It can be related to a dissipative potential (Φ) that represents the potential for energy loss due to the viscous effects in the material [53,57]. Mehrmashhadi et al. investigated the role played by the local heating around the crack-tip with peridynamics on the dynamic behaviour of PMMA [58] — a synthetic polymer that exhibits a viscoelastic behaviour [59,60]. However, their investigation does not consider a strain-rate dependent viscoelastic model although it takes into account heating at the crack-tip generated by the viscous dissipation.

Experimental evidence shows that resistance against failure of many rate-dependent materials decreases with temperature [41]. In viscoelastic materials, mechanical energy can be released through relaxation mechanisms [57]. This means that a portion of the strain energy that has been stored in the material can convert into heat, resulting in an increase in temperature. Hence, viscous dissipation can be assumed to promote fracture. Certain papers [35,36] incorporate the effects of viscous dissipation as heat into the free energy in order to promote fracture. This is achieved by introducing a factor ζ that represents the portion of viscous energy that ultimately promotes fracture. This approach provides a phenomenological account of the role of heat in viscoelastic dissipation as a promoter of fracture. The viscous energy can be split into two parts, one that is assumed to be a free energy, which corresponds to the portion that promotes fracture, and one that is dissipated (lost) to the surrounding, which corresponds to the portion that can neither be recovered nor produce work:

$$\begin{aligned} \underbrace{\Psi_v(\dot{\varepsilon}, d)}_{\text{viscous energy}} &= \underbrace{\zeta \Psi_v(\dot{\varepsilon}, d)}_{\text{free (irreversible)}} + \underbrace{(1-\zeta)\Psi_v(\dot{u}, d)}_{\text{dissipative (irreversible)}} \\ &= \zeta g(d)\bar{\Psi}_v(\dot{\varepsilon}) + (1-\zeta)g(d)\bar{\Psi}_v(\dot{\varepsilon}) \end{aligned} \tag{12}$$

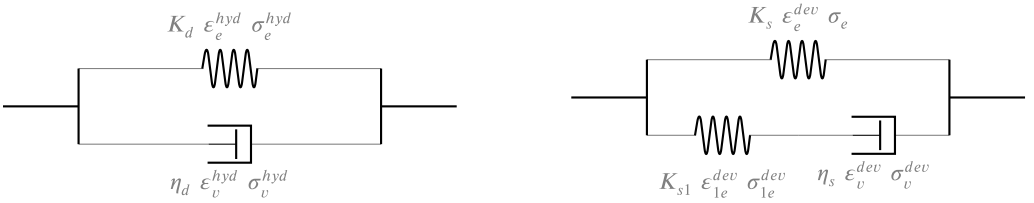

(a) Kelvin-Voigt model (hydrostatic) (b) Standard-linear model (deviatoric)

Fig. 2. Illustration of the viscoelastic model of the bulk: (b) Kelvin–Voigt model for the hydrostatic part and (a) Standard linear model for the deviatoric part.

$\bar{\Psi}_v$ corresponds to the intact viscous energy density, which can take any suitable form based on the considered model. It is assumed that both viscous and elastic properties are equivalently affected by damage, and both are degraded by the same degradation function $g(d)$, through which the coupling between the phase-field problem and the viscoelastic effects is possible. $\Psi_v = g(d)\bar{\Psi}_v(\dot{u}, d)$ can be understood as the viscous dissipation that has been accumulated in the presence of fracture [36]. When $\zeta = 0$, mechanical energy is lost in the bulk, and the effects of viscous dissipation do not foster fracture. On the other hand, when $\zeta = 1$, all of the viscous heat that is dissipated in the vicinity of the crack contributes to the softening of the material, and thus promotes damage formation.

The total free energy density of the phase-field problem in a viscoelastic material is written as [36]:

$$\begin{aligned}\underbrace{\Psi(\varepsilon,\dot{\varepsilon},d)}_{\text{free (stored)}} &= \underbrace{\Psi_e(\varepsilon,d)}_{\text{reversible}} + \underbrace{\zeta\Psi_v(\dot{\varepsilon},d)}_{\text{irreversible}} + \underbrace{\Psi_f(d,\nabla d)}_{\text{irreversible}} \\ &= g(d)\bar{\Psi}_e(\varepsilon,d) + \zeta g(d)\bar{\Psi}_v(\dot{\varepsilon}) + g_c\gamma_{l_c}\end{aligned} \tag{13}$$

When it comes to modelling viscoelastic materials, often, significant differences in the response between spheric and deviatoric deformations are generally observed [57,61]. In this paper, and in accordance with Luo et al. [62], a Kelvin–Voigt approach is employed to analyse the spheric portion of the stress–strain behaviour, as shown in Fig. 2(a), and a Maxwell-like model is utilised for the deviatoric part of the stress–strain behaviour, as illustrated in Fig. 2(b). This approach is grounded in the assumption that the viscous flow generated by the deviatoric component will be constrained by the solid's elasticity. And it is supported by the observation that the hydrostatic component primarily results in a delayed response without causing significant macroscopic flow, as described in Refs. [62,63].

In addition to the complete split between spheric and deviatoric components [62], this formulation displays another intriguing structure: a complete split between the elastic and the viscous components[1] :

$$\varepsilon = \varepsilon^{hyd} + \varepsilon^{dev} \tag{14a}$$

$$\sigma = \sigma^{hyd} + \sigma^{dev} \tag{14b}$$

$$\sigma^{hyd} = \sigma_e^{hyd} + \sigma_v^{hyd} \tag{14c}$$

$$\sigma^{dev} = \sigma_e^{dev} + \sigma_v^{dev}, \text{ which gives:} \tag{14d}$$

$$\sigma = \underbrace{\sigma_e^{hyd} + \sigma_e^{dev}}_{\text{elastic}} + \underbrace{\sigma_v^{hyd} + \sigma_v^{dev}}_{\text{viscous}} \tag{14e}$$

And the stresses can be formulated through a complete separation from both the elastic strain energy and the viscous energy as:

$$\sigma_e = \frac{\partial\Psi_e}{\partial\varepsilon} = \frac{\partial\Psi_e}{\partial\varepsilon_e} = g(d)\frac{\partial\bar{\Psi}_e}{\partial\varepsilon} \tag{15a}$$

$$\sigma_v = \frac{\partial\Psi_v}{\partial\varepsilon} = \frac{\partial\Psi_v}{\partial\varepsilon_v} = g(d)\frac{\partial\bar{\Psi}_v}{\partial\varepsilon} \tag{15b}$$

The superscript hyd corresponds to the hydrostatic stress σ and strain ϵ tensors. The superscript dev corresponds to the deviatoric stresses and strains. The subscripts e and v correspond to the elastic/viscous parts of the strains and stresses.

This structure will greatly improve the implementation of the energy-based rate-dependent phase-field method, as it allows for the clear separation of different energies based on their hydrostatic/deviatoric components, as well as whether they are dissipative or free energies.

[1] Interested readers are referred to Appendix for the full constitutive modelling of the viscoelastic bulk.

The total dissipated viscous energy $\bar{\Psi}_v$ at time t, which has been accumulated in the absence of fracture (intact), takes the following form as a function of the undamaged viscous stresses and strains:

$$\begin{aligned}\bar{\Psi}_v(t) &= \int_{-\infty}^{t} \bar{\sigma}_v : \dot{\varepsilon}_v d\tau = \int_{-\infty}^{t_n} \bar{\sigma}_v : \dot{\varepsilon}_v d\tau + \int_{t_n}^{t} \bar{\sigma}_v : \dot{\varepsilon}_v d\tau \\ &= \bar{\Psi}_v(t_n) + \int_{t_n}^{t} \bar{\sigma}_v : \frac{d\varepsilon_v}{d\tau} d\tau\end{aligned} \tag{16}$$

After introducing the general expression of the free energy in a viscoelastic solid (Eq. (13)) and elaborating on the impact of the choice of the viscoelastic model on the separation of the elastic and viscous energies, we give the strong form for the phase-field problem similarly to Eq. (8a):

$$\frac{\partial \Psi}{\partial d} = \frac{\partial g(d)}{\partial d}\bar{\Psi}_e + \zeta \frac{\partial g(d)}{\partial d}\bar{\Psi}_v + g_c \frac{\partial \gamma_{l_c}}{\partial d} = -2(1-d)(\bar{\Psi}_e + \zeta\bar{\Psi}_v) + g_c \frac{3}{8l_c}(1 - 2l_c^2 \Delta d) = 0 \quad \text{in } \Omega \tag{17a}$$

$$\nabla d \cdot n = 0 \quad \text{on } \partial\Omega \tag{17b}$$

$$\dot{d} \geq 0 \quad \text{in } \Omega \tag{17c}$$

The dissipation is written from the Clausius–Duhem inequality as:

$$\begin{aligned}\dot{D} &= \sigma : \dot{\varepsilon} - \dot{\Psi} \geq 0 \\ &= (\sigma_e + \sigma_v) : \dot{\varepsilon} - \Big(\frac{\partial \Psi}{\partial \varepsilon} : \dot{\varepsilon} + \underbrace{\frac{\partial \Psi}{\partial d}\dot{d}}_{0,\ \text{from Equation (17a)}} \Big) \\ &= \underbrace{\Big(\sigma_e - \frac{\partial \Psi_e}{\partial \varepsilon}\Big)}_{0} : \dot{\varepsilon} + \Big(\sigma_v - \zeta \frac{\partial \Psi_v}{\partial \varepsilon}\Big) : \dot{\varepsilon} \\ &= (\sigma_v - \zeta\sigma_v) : \dot{\varepsilon}_v \\ &= (1-\zeta)\sigma_v : \dot{\varepsilon}_v \geq 0\end{aligned} \tag{18}$$

$\sigma_v : \dot{\varepsilon}_v$ corresponds to the dissipation rate in the presence of damage, so naturally $\sigma_v : \dot{\varepsilon}_v \geq 0$. The above inequality stands for $\zeta \in [0, 1]$. And the thermodynamics consistency of such model is fulfilled.

Following the discussion of the phase-field formulation for viscoelastic materials, i.e., rate-dependency in the bulk, the next section focuses on the development of a phase-field model that incorporates a rate dependency of the fracture toughness for a rate-independent (elastic) bulk. First, the notion of the rate-dependency of the fracture toughness is previewed.

2.2. Strain-rate dependent fracture toughness

It was postulated theoretically [44,45] and observed experimentally [64,65] that the fracture toughness of most materials (even brittle ones) increases when the crack accelerates. This strain-rate effect is also commonly found in civil engineering structures and in polymeric materials. In the latter, the rate-dependent effects can be explained by the following: when fast loading is applied, the external energy required to break the material is higher, since the chemical bonds of the chains have to break (orange links in Fig. 3(a)). In contrast, for slow loading, the chain segments can rearrange and torn out of the matrix which requires a lower level of energy in order to be broken (blue chains in Fig. 3(a)) [35,48]. For instance, Sharon et al. [66] report a strong increase of the fracture energy with the crack velocity in PMMA. They show that fracture energy ranges from approximately 1000 J/m^2 at a crack-tip velocity $v_c = 0.2c_R$ up to 8000 J/m^2 at $v_c = 0.68c_R$. Quasi-static experiments on PMMA usually report values of fracture energy in the range of 300–400 J/m^2 [67]. This highlights the fact that dynamic behaviour of such materials is indeed complex, and that rate-dependency is a necessity to accurately model their behaviour.

Approaches considering crack-velocity-dependent fracture toughness, that assume that fracture toughness would increase accordingly to the tip speed are available [44,68]. However, the uniqueness of the relation between crack velocity and the fracture toughness is questionable [45]. Yet, there is still no consensus on the manner. For instance, Özenç [68] implements the following expression for discrete crack approximation:

$$g_c = g_{c0}\left[1 + \left(\frac{v_c}{c_\infty}\right)^\beta\right] \tag{19}$$

Here, g_{c0} is the quasi-static value of the fracture toughness, c_∞ is a reference crack propagation velocity. c_∞ can be taken equal to the theoretically limiting Rayleigh wave-speed c_R. β is an amplification factor whose influence is illustrated in Fig. 3(b).

When using the phase-field continuous method instead of discrete crack approximations, obtaining and measuring the instantaneous crack-propagation velocity is challenging. This is because the crack is represented by a damage band of finite width, making it difficult to determine the exact crack-tip positions. Inaccurate predictions of crack-tip positions can then lead to incorrect velocity calculations, particularly for dynamic fracture. But most importantly, how could the material know locally, how should the toughness be modified based on a globally observed/measured quantity (v_c)?

The consideration of a strain-rate dependent toughness seemed a flexible and natural choice by Yin et al. [46]. The availability of the deformation rate in continuous simulations, and the observations that link the strain-rates around the crack-tip to post-processed

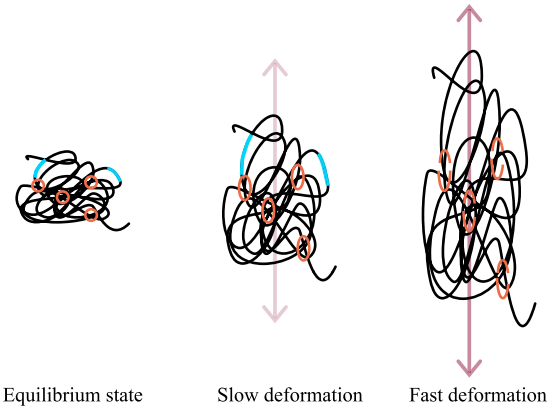

(a) Underlying mechanisms of the rate-dependent toughness in polymers

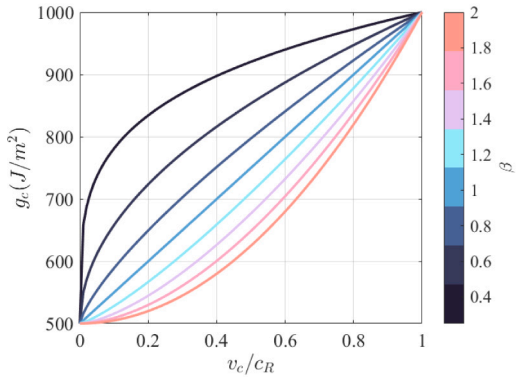

(b) Influence of the amplification factor on the rate-dependent toughness

Fig. 3. Rate-dependent toughness: the underlying mechanisms (a) in polymers and the influence of the amplification factor (b) — Eq. (19).

crack-tip speeds, allows accounting for the crack-velocity-dependent fracture toughness through a strain-rate dependency. In the following, we tackle the phase-field formulation of fracture in an elastic material with strain-rate dependent toughness.

Yin et al. [46] assume that fracture toughness would quadratically increase accordingly to the rate of the strain tensor, and that the static fracture toughness would be recovered at small strain-rates. The instantaneous toughness is written as [46]:

$$g_c(\dot{\epsilon}) = g_{c0}(1 + \tau_\epsilon^2 \, \dot{\epsilon} : \dot{\epsilon}) \tag{20}$$

where τ_ϵ is a characteristic time that would specify the amount of the strain-rate dependency of the fracture toughness. Unlike in Ref. [46], here, it is assumed that the rate-dependent fracture toughness depends on the rate of the strain independently on whether it is a compressive or a tensile rate, since the configuration to be analysed here is primarily tensile-stress dominant and no crack closure is modelled. Moreover, if the material is in compression, a modification of the fracture toughness g_c would have no effect on its behaviour, since the spectral split of the strain energy would prohibit damaging. Yin et al. [46] also add a degradation function that multiplies τ_ϵ to basically prevent an increase of the fracture toughness in the damaged regions. However, it is believed that the degradation of the material limits the strain-rates in the damaged regions and naturally prevents the undesired increase in the fracture toughness in the already-damaged region. Of course, the consideration of a quadratic model (Eq. (20)) does not guarantee a higher limit on the toughness which may not be accurate according to some experimental findings [47]. Knowingly, multiple efforts were made to suggest different functions relating the fracture toughness to the strain-rate with the sigmoid-shaped function proposed by Miehe et al. [33] and followed by Dammaßet al. [48]. However, this adds to the complexity of the implementation. We will be restricted to the used of the strain-rate dependency of the toughness as given in Eq. (20).

The incorporation of strain-rate dependency of the fracture toughness into the phase-field model of fracture yields the following expression for total free energy:

$$\begin{aligned}\underbrace{\Psi(\varepsilon,\dot{\varepsilon},d)}_{\text{free (stored)}} &= \underbrace{\Psi_e(\varepsilon,d)}_{\text{reversible}} + \underbrace{\Psi_f(\dot{\varepsilon},d,\nabla d)}_{\text{irreversible}} \\ &= g(d)\bar{\Psi}_e(\varepsilon) + g_c(\dot{\varepsilon})\gamma_{l_c} \\ &= g(d)\bar{\Psi}_e(\varepsilon) + g_{c0}(1+\tau_\varepsilon^2\,\dot{\varepsilon}:\dot{\varepsilon})\gamma_{l_c}\end{aligned} \tag{21}$$

We give the strong form for the phase-field problem of fracture in an elastic material with strain-rate dependent toughness:

$$\frac{\partial\Psi}{\partial d} = \frac{\partial g(d)}{\partial d}\bar{\Psi}_e + g_c\frac{\partial\gamma_{l_c}}{\partial d} = -2(1-d)\bar{\Psi}_e + g_{c0}(1+\tau_\varepsilon^2\dot{\varepsilon}:\dot{\varepsilon})\frac{3}{8l_c}(1-2l_c^2\Delta d) = 0 \qquad \text{in } \Omega \tag{22a}$$

$$\nabla d\cdot n = 0 \qquad \text{on } \partial\Omega \tag{22b}$$

$$\dot{d} \geq 0 \qquad \text{in } \Omega \tag{22c}$$

Here, the fracture energy term encloses a strain dependency, more specifically, a strain-rate dependency. A linear approximation of the temporal discretisation yields the following strain rates:

$$\dot{\varepsilon}(t=t_{n+1}) \simeq \frac{\varepsilon(t_{n+1})-\varepsilon(t_n)}{\Delta t} \tag{23}$$

From here, the rate of internal dissipation can be approximated within an infinitesimal time step Δt, with the consideration of an additional internal variable corresponding to the strain-rate tensor at a previous time step. It reads:

$$\begin{aligned}\dot{D} &= \sigma:\dot{\varepsilon} - \dot{\Psi} \geq 0 \\ &\simeq \sigma:\dot{\varepsilon} - \left(\frac{\partial\Psi}{\partial\varepsilon(t_{n+1})}:\dot{\varepsilon}(t_{n+1}) + \frac{\partial\Psi}{\partial\varepsilon(t_n)}:\dot{\varepsilon}(t_n) + \cancelto{0,\text{ from Equation (22a)}}{\frac{\partial\Psi}{\partial d}\dot{d}}\right) \\ &= \underbrace{\left(\sigma - \left(\frac{\partial\Psi_e}{\partial\varepsilon(t_{n+1})} + \frac{\partial\Psi_f}{\partial\varepsilon(t_{n+1})}\right)\right)}_{0}:\dot{\varepsilon}(t_{n+1}) - \frac{\partial\Psi_f}{\partial\varepsilon(t_n)}:\dot{\varepsilon}(t_n)\end{aligned} \tag{24}$$

Evaluating the total Cauchy stress from Eq. (24) gives a viscous-like stress term that contributes to the total stresses:

$$\begin{aligned}\sigma &= \frac{\partial\Psi_e}{\partial\varepsilon(t_{n+1})} + \frac{\partial\Psi_f}{\partial\varepsilon(t_{n+1})} \\ &= g(d)\frac{\partial\bar{\Psi}_e}{\partial\varepsilon} + \frac{\partial g_c(\dot{\varepsilon})}{\partial\varepsilon}\gamma_{l_c} \\ &= g(d)\frac{\partial\bar{\Psi}_e}{\partial\varepsilon} + \frac{\partial[g_{c0}(1+\tau_\varepsilon^2\dot{\varepsilon}:\dot{\varepsilon})]}{\partial\varepsilon}\gamma_{l_c} \\ &= g(d)\frac{\partial\bar{\Psi}_e}{\partial\varepsilon} + g_{c0}\tau_\varepsilon^2\gamma_{l_c}\frac{\partial(\dot{\varepsilon}:\dot{\varepsilon})}{\partial\varepsilon} = \sigma_e + \sigma_f\end{aligned} \tag{25}$$

σ_f is the viscous-like stress term contributing to the total stresses and inherent to the strain-rate-dependency of the toughness, it can be rewritten as:

$$\begin{aligned}\sigma_f &= g_{c0}\tau_\varepsilon^2\gamma_{l_c}\frac{\partial(\dot{\varepsilon}:\dot{\varepsilon})}{\partial\varepsilon} \\ &= g_{c0}\tau_\varepsilon^2\gamma_{l_c}\frac{\partial(\dot{\varepsilon}:\dot{\varepsilon})}{\partial\dot{\varepsilon}}:\frac{\partial\dot{\varepsilon}}{\partial\varepsilon} \\ &= g_{c0}\tau_\varepsilon^2\gamma_{l_c}2\dot{\varepsilon}:\frac{\partial\dot{\varepsilon}}{\partial\varepsilon}\end{aligned} \tag{26}$$

Following the linear approximation of the temporal discretisation, the viscous-like stress σ_f can be approximated by:

$$\begin{aligned}\sigma_f &= g_{c0}\tau_\varepsilon^2\gamma_{l_c}2\dot{\varepsilon}:\frac{\partial\dot{\varepsilon}}{\partial\varepsilon} \\ &\simeq g_{c0}\tau_\varepsilon^2\gamma_{l_c}2\dot{\varepsilon}\frac{1}{\Delta t}\end{aligned} \tag{27}$$

And the additional term in the dissipation in Eq. (24) reads:

$$\begin{aligned}\dot{D} = -\frac{\partial\Psi_f}{\partial\varepsilon(t_n)}\dot{\varepsilon}(t_n) &= g_{c0}\tau_\varepsilon^2\gamma_{l_c}\frac{1}{\Delta t}2\dot{\varepsilon}(t_{n+1}):\dot{\varepsilon}(t_n) \\ &\simeq g_{c0}\tau_\varepsilon^2\gamma_{l_c}\frac{1}{\Delta t}2\dot{\varepsilon}(t_{n+1}):\dot{\varepsilon}(t_{n+1}) \geq 0\end{aligned} \tag{28}$$

This thermodynamically-consistent dissipation rate is related to the viscous-like strains inherent to the strain-rate dependency of the toughness in the phase-field model. Next, we describe the formulation of the phase-field model of fracture in an elastic material with damage-rate dependent toughness.

2.3. Damage-rate dependent fracture toughness

Alternatively to the strain-rate dependent toughness model, we propose a model that relates the fracture toughness to the rate of damage at the crack-tip. The motivation behind this choice is discussed later, in Section 3.1. A linear model is proposed to link the toughness around the crack tip to the damage rate:

$$g_c(\dot{d}) = g_{c0}(1 + \tau_d\ \dot{d}) \tag{29}$$

Here, τ_d relates to a characteristic time that determines the amount of damage-rate-dependency of the fracture toughness. As the damage converges to the value $d = 1$, its rate tends to zero and the static value of the toughness should be recovered. At the crack-tip, the damage rate is found to increase linearly with the crack-tip velocity, while a quadratic evolution is observed for the strain-rates as a function of the crack-tip velocity (Section 3.1). Further, we note that, unlike the strain rates, the damage rates around the crack tip do not decline as the crack widens (Section 3.1); this further demonstrates the robustness of such a formulation – as compared to a strain-rate dependent toughness formulation – to account for the crack-velocity-dependency of the fracture.

The incorporation of damage-rate dependency of the fracture toughness into the phase-field model of fracture yields the following expression for total free energy:

$$\begin{aligned}\underbrace{\Psi(\varepsilon,d)}_{\text{free (stored)}} &= \underbrace{\Psi_e(\varepsilon,d)}_{\text{reversible}} + \underbrace{\Psi_f(\dot{d},d,\nabla d)}_{\text{irreversible}} \\ &= g(d)\bar{\Psi}_e(\varepsilon,d) + g_c(\dot{d})\gamma_{l_c} \\ &= g(d)\bar{\Psi}_e(\varepsilon,d) + g_{c0}(1+\tau_d\ \dot{d})\gamma_{l_c}\end{aligned} \tag{30}$$

The strong form for the phase-field problem for an elastic material with a damage-rate dependent fracture toughness reads:

$$\begin{aligned}\frac{\partial\Psi}{\partial d} &= \frac{\partial g(d)}{\partial d}\bar{\Psi}_e + g_c\frac{\partial\gamma_{l_c}}{\partial d} + \frac{\partial g_c}{\partial d}\gamma_{l_c} \\ &= -2(1-d)\bar{\Psi}_e + g_{c0}(1+\tau_d\dot{d})\frac{3}{8l_c}(1-2l_c^2\Delta d) + g_{c0}\tau_d\frac{\ddot{d}}{\dot{d}}\frac{3}{8l_c}(d + l_c^2\nabla d\cdot\nabla d) = 0 \quad \text{in } \Omega\end{aligned} \tag{31a}$$

$$\nabla d\cdot n = 0 \qquad \text{on } \partial\Omega \tag{31b}$$

$$\dot{d} \geq 0 \qquad \text{in } \Omega \tag{31c}$$

Following the linear approximation of the temporal discretisation, the following damage rates can be yielded:

$$\dot{d}(t = t_{n+1}) \simeq \frac{d(t_{n+1}) - d(t_n)}{\Delta t} \tag{32}$$

And the rate of internal dissipation can be approximated within an infinitesimal time step Δt with the consideration of an additional internal variable corresponding to the damage variable at a previous time step (t_n). The dissipation reads:

$$\begin{aligned}\dot{D} &= \sigma : \dot{\varepsilon} - \dot{\Psi} \geq 0 \\ &= \sigma : \dot{\varepsilon} - \left(\frac{\partial\Psi}{\partial\varepsilon(t_{n+1})}\dot{\varepsilon}(t_{n+1}) + \frac{\partial\Psi}{\partial d(t_n)}\dot{d}(t_n) + \cancel{\frac{\partial\Psi}{\partial\dot{d}(t_{n+1})}\dot{d}(t_{n+1})}^{\,0,\ \text{from Equation (31a)}}\right) \\ &= \underbrace{\left(\sigma - \frac{\partial\Psi_e}{\partial\varepsilon(t_{n+1})}\right)}_{0} : \dot{\varepsilon}(t_{n+1}) - \frac{\partial\Psi_f}{\partial d(t_n)}\dot{d}(t_n)\end{aligned} \tag{33}$$

The additional dissipation term is related to the damage-rate dependency of the fracture toughness appears:

$$\begin{aligned}\dot{D} &= -\frac{\partial\Psi_f}{\partial d(t_n)}\dot{d}(t_n) = g_{c0}\frac{\tau_d\gamma_{l_c}}{\Delta t}\dot{d}(t_n) \\ &\simeq g_{c0}\frac{\tau_d\gamma_{l_c}}{\Delta t}\dot{d}(t_{n+1}) \geq 0\end{aligned} \tag{34}$$

Remark 2. When considering rate-dependent toughness, and if a viscoelastic bulk is to be considered, the total dissipation is the summation of the dissipation related to the viscous strains (viscoelastic dissipation — Eq. (18)) and the dissipation related to the rate dependent toughness — Eqs. (28) or (34).

3. Crack-tip velocities in rate-dependent materials

We conduct a numerical study on the dynamic fracture response of various rate-dependent materials on a uniform displacement strip configuration [5,50,51]. The implementation was carried out in Abaqus [56,69].

The uniform displacement strip draws inspiration from the earlier studies of Refs. [49,50], which involved a steady crack growing at a velocity v_c in a homogeneous and isotropic elastic thin strip of width $2H$. In these studies, the edges of the strip were subjected to a uniform normal displacement u_0. The current configuration also incorporates the findings of recent experimental and numerical investigations by Corre et al. [10] and Kamasamudram et al. [14].

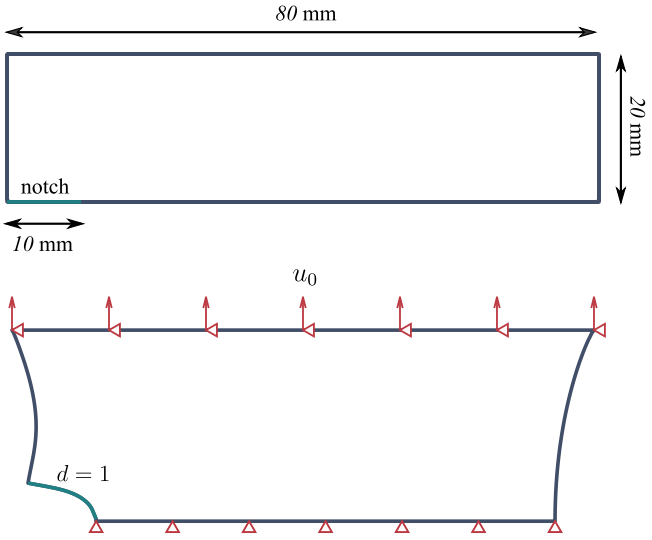

Fig. 4. Half-strip geometry (top) and applied boundary conditions (bottom) for the uniform displacement strip.

Here, only half the specimen will be modelled. The half-strip geometry and the applied boundary conditions are shown in Fig. 4. The dimensions of the specimen are $L = 80$ mm for length and $H = 20$ mm for half-width. Unlike the procedure followed in Refs. [10,14], our model has a pre-existing crack of length $a = 10$ mm. This crack is represented both geometrically and through the imposed Dirichlet boundary condition $d = 1$ (fully broken) on the initial crack surface. The specimen is pre-strained by applying uniform displacements u_0 in the vertical direction on the top surface, and the bottom surface is held fixed in the vertical direction (Fig. 4). During the pre-strain step, the top is loaded statically (without the effect of inertia) to reach the target value u_0; the damaging is deactivated. In this step, the evolution of damage is disabled in order to model dynamic crack growth later on. If damage were to be applied during the static pre-stretch, the crack would initiate much earlier than the target value, due to the additional dissipation (energy release rate) required for dynamic crack propagation [50,70]. After the target displacement is reached, the damage phase-field is activated and the crack initiates from the notch.

The specimen is discretised by 36 472 four-node bilinear plane-strain quadrilateral elements and the mesh is refined to a size $h_m = 0.1$ mm in the region where the crack is expected to evolve. As mentioned by Bleyer et al. [5], the herein considered configuration closely resembles the infinite strip configuration [50], in which a steady-state propagation occurs with a fracture energy equivalent to the initially stored strain–energy. This makes this configuration appropriate to analyse velocity-dependent and rate-dependent fracture phenomena.

3.1. Rate-independent model

We first investigate the configuration with the classical rate-independent phase-field model. Table 1 resumes the overall model and material parameters considered in the rate-independent simulations. For an imposed displacement of $u_0 = 0.0741$ mm, the corresponding damage evolution and the crack-tip speed of the main crack are shown in Fig. 5. The crack is initiated with a tip-speed of $v_c = 400$ m/s. Initially, an elastic energy ($\simeq Eu_0^2 L/H$) is stored in the system due to the static loading [5,50]. Once the damage is activated, this energy is to be instantly released and a crack initiates with a non-null initial tip speed $v_c = 400$ m/s. This non-zero initial crack-tip velocity is also observed in a similar configuration reported in Ref. [5]. The profile of the phase-field crack starts to broaden as the tip speed reaches $v_c = 500$ m/s. The crack accelerates to a limiting velocity below the Rayleigh wave speed $v_c = 640$ m/s $\simeq 0.72 c_R$. A small drop in velocity is observed and sequentially an independent branch appears [9,26]. The velocity of the Rayleigh waves is given by Freund [50] as:

$$c_R = c_s \frac{0.862 + 1.14\nu}{1 + \nu}, \tag{35}$$

where c_s is the shear wave-speed $c_s = \sqrt{K_s/\rho}$, and K_s is the shear modulus. The velocity limit herein obtained is in good correspondence with the theoretical limit related to the Rayleigh wave speed [2,9,50,71]. It is also in good correspondence with limiting velocities found in previous experimental studies [51], phase-field simulations [5], and numerical investigations of the continuum damage models [25,26].

Remark 3. The crack-tip speed is computed by differentiating the positions of the crack tip in time. The position of the main crack tip is calculated as the largest extension in the horizontal direction of the iso-value of the nodal phase-field $d = 0.9$. The crack-tip velocity hence corresponds to the horizontal component of the instantaneous velocity vector of the crack tip. As we focus on the

Table 1
Overall damage phase-field model and material parameters for the rate-independent simulation.

E (Young's modulus)	3 GPa
ν (Poisson's ratio)	0.35
ρ (Mass density)	1200 kg/m^3
g_c (Static fracture toughness)	500 J/m^2
l_c (Length-scale parameter)	400 μm
Crack density function	Linear (AT1)
Strain split	Spectral decomposition
Plane strain assumption	
Time integration	implicit (HHT) [72]
Δt_c (time step)	10^{-5} ms
h_m (refined mesh size)	$l_c/4 = 100$ μm

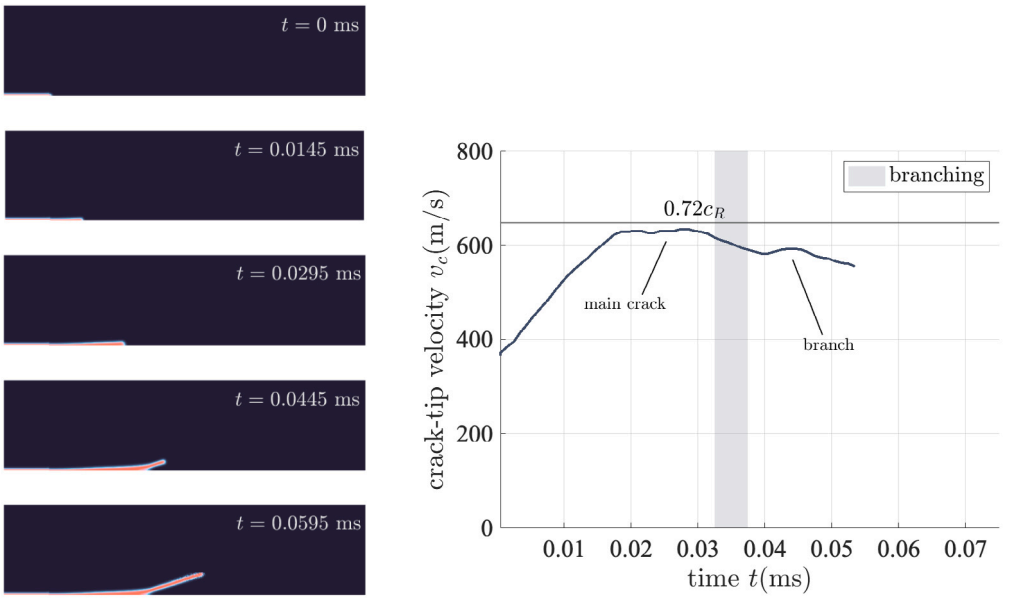

(a) Fracture patterns at different time steps (b) Crack-tip speed of the main branch

Fig. 5. Uniform displacement strip results (imposed vertical displacement $u_0 = 0.0741$ mm) for rate-independent the material.

limiting crack-tip velocities, only the main crack is followed in Sections 3.2, 3.3, 3.4. In the case of branching, the velocities of the branches are not reported.

Since the strain and damage rates would constitute the main ingredients for the rate-dependent model of the fracture toughness , we investigate the evolution of these quantities around the crack-tip for different imposed displacements u_0 in the rate-independent configuration. More specifically, we analyse their evolution with the crack-tip velocity.

We report the maximum value of the rate of the largest principal strain (tensile) and the maximum value of the rate of the damage in a confined region of size $2 \times l_c$ around the crack-tip. The evolution of the strain and the damage rates as a function of the crack-tip velocity at different imposed displacements are reported in Fig. 6. It is noted that for an imposed displacement $0.05643 \leq u_0 \leq 0.06056$ mm, a widening of the damage band is observed, for $u_0 = 0.0741$ mm, crack branching (preceded by crack widening) occurs.

For crack-tip speeds $0 \leq v_c \leq 500$ m/s, a monotonic relationship is found between both the strain and damage rate on one side, and the crack-tip velocity on the other. A quadratic relationship is found between the strain rates and the crack-tip velocity, as shown in Fig. 6(a), while a linear relationship is found between the damage rate and the crack-tip velocity, as shown in Fig. 6(b). However, at high crack-tip speeds ($v_c > 500$ m/s), none of these relationships stand. While the strain rates drop after reaching a maximum value around $v_c = 500$ m/s as the crack starts widening, the damage-rates continue with their monotonic evolution but at a slower rate. At the crack's limiting velocity $v_c = 640$ m/s, both the strain and damage rates drop significantly.

We believe that as crack widening and crack branching (usually preceded by widening [5,9]) occur, the strains are no longer localised at the tip, and as a consequence their rate would significantly drop as they become more diffused. This is exactly what is shown for $u_0 = 0.0741$ mm in Figs. 5(a) and 6(a). Once the crack reaches a tip-speed of $v_c = 500$ m/s, which is around $t = 0.01$ ms, we

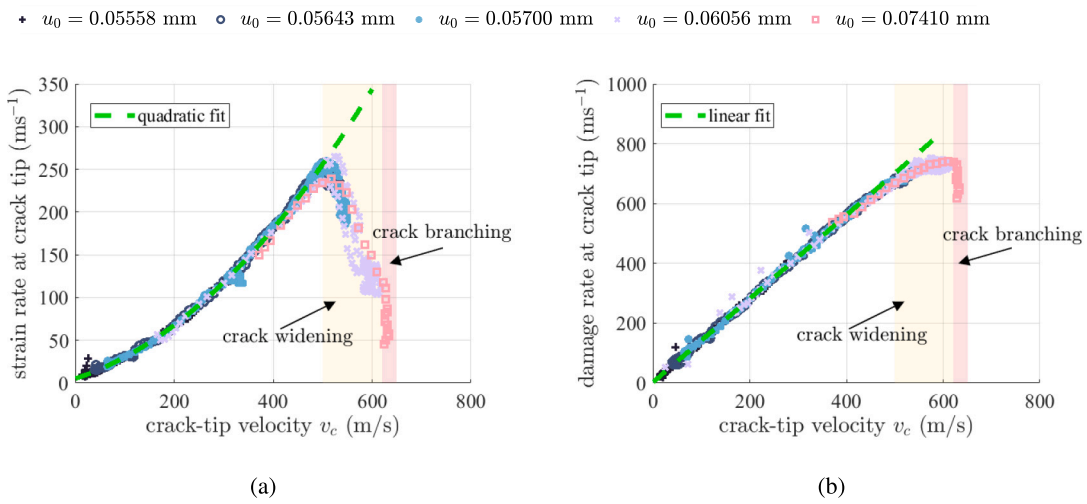

Fig. 6. The evolution of the strain and the damage rates around the crack tip as a function of the crack-tip velocity. A quadratic relationship is found between the strain rates and the tip velocities (a). A linear relationship is found between the damage rates and the tip velocities (b).

can see how the damage-band begins to widen (Fig. 5(a)) and parallelly, the rate of the strains begins to drop. However, this is not the case for the damage rates. If the strain-rate drops as the crack-tip speed reaches $v_c = 500$ m/s and the damage band widens, the damage-rate keeps increasing until the crack-tip velocity reaches its limiting value around $v_c = 640$ m/s before branching occurs.

As per Bleyer et al. [5], crack branching can be viewed as a consequence of an excess of available energy flowing to the crack tip which cannot be dissipated by a single crack propagation. From here, we believe that the rate at which a crack surface is formed, as the widening of the crack occurs, need not to drop in order for the excess energy to be dissipated, equivalently, the damage-rate need not to drop, although a small decline can be expected especially as two crack-tips co-exist after the branching phenomenon (Fig. 6).

To resume, unlike the strain rates, the damage rates around the crack tip do not decline as the crack widens. The formulation of a damage-rate dependent (linear) toughness model appears a flexible choice to carefully account for the crack-velocity-dependency of the fracture, of course besides the existing strain-rate dependent formulation [46].

3.2. Viscoelasticity

In order to discuss the consequences of the different rate-dependent modelling assumptions, multiple simulations are explored for the same imposed vertical displacement $u_0 = 0.0741$ mm. First, the effect of the viscoelasticity of the bulk is analysed (Section 3.2), followed by the effect of a strain-dependent (Section 3.3) and damage-dependent toughness (Section 3.4) with a rate-independent bulk. The results are compared to the rate-independent simulation (Section 3.1).

To perform the analysis on viscoelastic strips, we use the phase-field parameters listed in Table 1. For the viscoelastic model, the required shear and bulk moduli are the plane-strain equivalent moduli of the elastic properties (E and ν) found in Table 1. Only the viscosity of the strips is altered, no rate-dependency of the toughness is considered. Materials with different relaxation times – 0 (elastic) $\leq \tau_v \leq 2.5 \cdot 10^{-4}$ ms – are analysed to put forth the role played by the viscosity of the bulk on the dynamic fracture behaviour. Both shear and bulk viscosities (η_s and η_d) are assumed to have equivalent values. To compare the influence of the viscous effects, the results are contrasted regarding the materials' relaxation times $\tau_v = \tau_{vd}$. Only the viscoelastic properties that yielded the most compelling results are exhaustively reported ($\tau_v = 0$, 10^{-7}, $7.5 \cdot 10^{-6}$, $8.75 \cdot 10^{-6}$, 10^{-5}, $7.5 \cdot 10^{-5}$ and $2.5 \cdot 10^{-5}$ ms).

Regarding the contribution of the viscoelastic dissipation to the fracture process (through the factor ζ), the two most prominent cases are considered :

1. The heat produced by the viscous dissipation in the bulk does not promote fracture, i.e., $\zeta = 0$; the corresponding results are shown in Fig. 7.
2. The heat produced by the viscous dissipation in the bulk does promote fracture and the entirety of the viscous energy will contribute to the fracture, i.e., $\zeta = 1$; the corresponding results are shown in Fig. 8.

3.2.1. Viscoelasticity with $\zeta = 0$

Fig. 7(a) shows the crack path in the fine-mesh region with respect to the characteristic time (τ_v) for $\zeta = 0$. Generally, the main crack is initiated from the notch. A broadening of the damage-band is observed in the materials with the characteristic times $\tau_v = 0$, 10^{-7}, $7.5 \cdot 10^{-6}$, $8.75 \cdot 10^{-6}$ and 10^{-5} ms. Crack branching occurs in the materials with the characteristic times $\tau_v = 0$, 10^{-7} and $7.5 \cdot 10^{-6}$ ms. With the increase of the characteristic time of the material – through increasing the values of the viscous properties

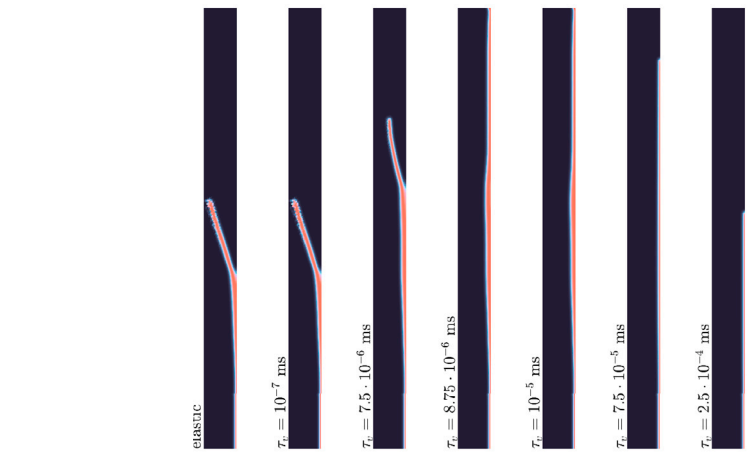

(a) Fracture patterns

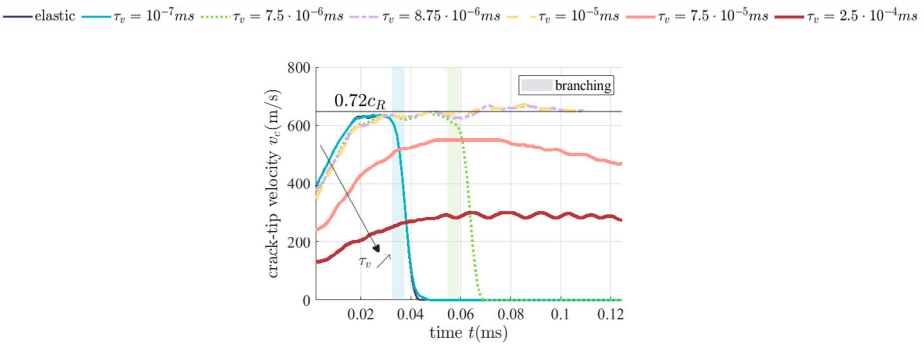

(b) Crack-tip velocities

Fig. 7. Viscoelastic materials with different characteristic times τ_v and $\zeta = 0$: uniform displacement strip results at $u_0 = 0.0741$ mm.

– both the crack widening and the crack branching phenomena appear after longer paths travelled by the initial cracks. Starting τ_v around $8.75 \cdot 10^{-6}$ ms, although the widening of the damage-band still appears, the branching phenomenon is suppressed. As the viscosity is further increased, both the branching and the damage-band widening disappear. Furthermore, the final crack topology shows a shorter crack path.

Regarding the crack tip speeds shown in Fig. 7(b), in all cases, the cracks are instantly initiated at different initial tip speeds v_c depending upon the viscous properties of the materials (the characteristic times). As the dynamic phase-field fracture is activated, and fracture is initiated at the notch, the strain-rates are the larger and so is the viscous dissipation. An increased value of τ_v translates to an increase in the mechanical dissipation, and this is directly reflected on the initial crack-tip speeds.

The cracks then accelerate towards a plateau value. Both the acceleration and the plateau value are dependent on the viscoelastic parameters. The acceleration decreases as the energy valuable for the crack decreases, and this phenomenon is coherent with theoretical considerations for the similar configuration [50]. In the cases where the crack branches, similar values of the plateau $v_c \simeq 640$ m/s are reached before the branching phenomenon. At $\tau_v = 8.75 \cdot 10^{-6}$ and 10^{-5} ms, after the first plateau, and as no branching occurs, the crack re-accelerates to reach a slightly higher plateau at $v_c \simeq 670$ m/s and surpasses the previously obtained velocity ($\simeq 640$ m/s). As the viscosity is further increased, the values of the plateaus decrease. As the mechanical dissipation increases, a smaller value of the phase-field is perceived as the driving force (elastic strain–energy) decreases. In its turn, this decrease results in a slower crack, thus, lowering the possibility of branching around the widened region of the damage-band. This explains the longer distance the crack needed to propagate before widening/branching with significant viscosities τ_v. It also explains the total suppression of the branching as the tip speeds decrease with the further increase of the viscosities.

3.2.2. *Viscoelasticity with* $\zeta = 1$

Fig. 8(a) shows the crack path in the fine-mesh region with respect to the characteristic time of the viscoelastic material in which the viscous dissipation in the bulk promotes fracture in its entirety ($\zeta = 1$). Generally, the main crack is instantly initiated from the notch. A broadening of the damage-band is observed in the materials with the characteristic times $\tau_v = 0$, 10^7, $7.5 \cdot 10^{-6}$, $8.75 \cdot 10^{-6}$ and 10^{-5} ms. Unlike in the case where $\zeta = 0$, here it is assumed that the viscous dissipation does promote fracture. This

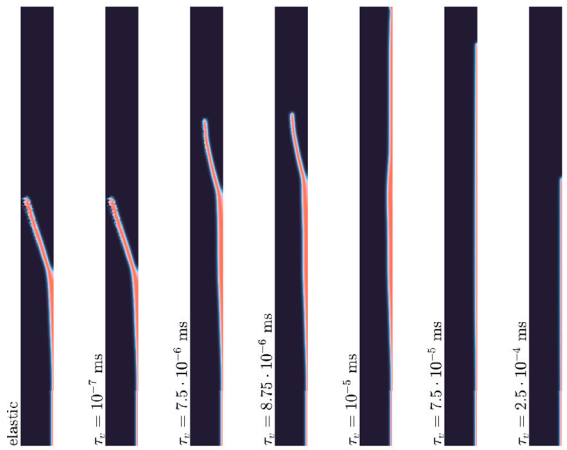

(a) Fracture patterns

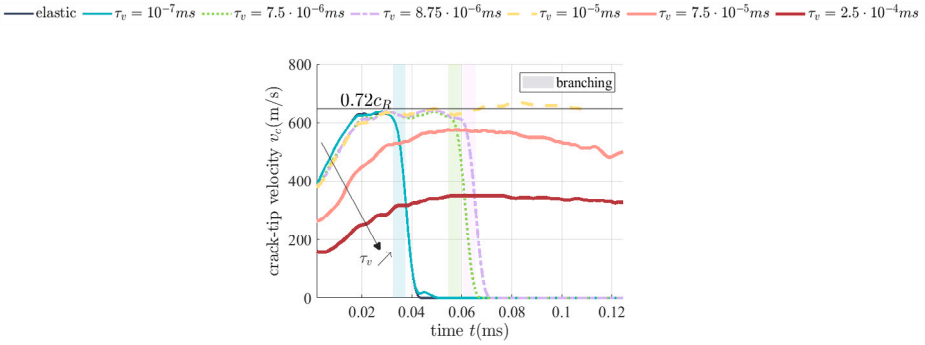

(b) Crack-tip velocities

Fig. 8. Viscoelastic materials with different characteristic times τ_v and $\zeta = 1$: uniform displacement strip results at $u_0 = 0.0741$ mm.

assumption directly translates to the fracture phenomena observed in the simulations, as crack branching occurs in the materials with the characteristic times $\tau_v = 0$, 10^{-7}, $7.5 \cdot 10^{-6}$ but also at $\tau_v = 8.75 \cdot 10^{-6}$ ms, which was not the case for $\zeta = 0$. Indeed, a viscous contribution to fracture can essentially trigger a branching that is not predicted in viscoelastic materials if only strain energy is assumed to drive fracture [35]. Similarly to the case $\zeta = 0$, with the increase of the characteristic time of the material, both the crack widening and the crack branching appear only after the crack had travelled longer paths. At τ_v around 10^{-5} ms, the branching phenomenon is suppressed even though the damage-band appears to broaden. As the viscosity is further increased, in addition to the suppression of the branching and the damage-band widening, the final crack path shows a shorter crack path.

Regarding the crack tip speeds shown in Fig. 8(b), in all cases, the cracks are initiated at initial tip speeds v_c that depend upon the viscoelastic properties of the materials. The cracks then accelerate towards a plateau value. Both the acceleration and the plateau value are dependent on the viscoelastic parameters and hence the viscous dissipation at the notch and in the bulk. The acceleration decreases as the energy valuable for the crack decreases, and this phenomenon is coherent with theoretical considerations for the similar configuration [50]. In the cases in which the crack-branches, similar values of the plateau $v_c \simeq 640$ m/s are reached before branching. This value is similar to the one observed in the rate-independent simulation and in the viscoelastic case where $\zeta = 0$. At $\tau_v = 10^{-5}$ ms, after the plateau, and as no branching occurs, the crack re-accelerates to reach a slightly higher value of $v_c \simeq 670$ m/s and surpasses the previous attained velocity ($\simeq 640$ m/s). As the viscosity in the bulk is further increased, the plateaus values also decrease; however, their values are slightly higher than the ones reached in the case of $\zeta = 0$. This can be explained by the following: the higher the viscous effects, the more mechanical energy is dissipated and the larger the driving force is for the fracture through the factor ζ.

To resume, the simulations show how the viscoelasticity of the bulk highly influences the dynamic behaviour of fracture. Whether the viscous dissipation promotes fracture or not, the influence of viscoelasticity in suppressing the crack-branching and potentially accelerating the crack tip were put forth. And since the damaging process depends on the available free energy, the viscous dissipation is shown to play a major role in the dynamic fracture process.

3.3. Strain-rate dependent fracture toughness

To analyse the influence of the strain-rate dependent toughness on the dynamic crack propagation, a rate-independent (elastic) bulk is considered. The material properties and phase-field parameters are the same as the ones found in Table 1. Regarding the rate-dependent fracture toughness, its static value g_{c0} is considered to be equal to the fracture toughness of the rate-independent material from Table 1, so: $g_{c0} = 500$ J/m^2. Simulations are explored for the same imposed vertical displacement $u_0 = 0.0741$ mm. In this example we analyse materials with varying levels of rate-dependent toughness, ranging from a minimum of $\tau_\epsilon = 0$ ms (rate-independent) to a maximum of $\leq 3.2 \cdot 10^{-3}$ ms (for details, see Eq. (20) in Section 2.3).

Only the characteristic times that yielded the most compelling results are exhaustively reported ($\tau_\epsilon = 0$, 10^{-4}, $3.162 \cdot 10^{-4}$, $7.071 \cdot 10^{-6}$, 10^{-3}, $2.236 \cdot 10^{-3}$ and $3.162 \cdot 10^{-3}$ ms).

Fig. 9(a) shows the crack path in the fine-mesh region with respect to the characteristic time τ_ϵ. A clear broadening of the damage-band is observed in the materials with the characteristic times $\tau_\epsilon = 0$, 10^{-4}, $3.162 \cdot 10^{-4}$ and $7.071 \cdot 10^{-4}$ ms. Even for the larger characteristic times $\tau_\epsilon = 10^{-3}$, $2.236 \cdot 10^{-3}$ and $3.162 \cdot 10^{-3}$ ms, the damage-band is wider than $2l_c$ which was not the case in the viscoelastic materials (Section 3.2). Crack branching occurs in the materials with the characteristic times $\tau_\epsilon = 0$, 10^{-4} and $3.162 \cdot 10^{-4}$ ms. As the characteristic time of the material increases, the rate-dependency of its fracture toughness g_c also increases. This leads to crack widening and branching phenomena occurring after only the cracks have travelled longer distances. At τ_ϵ around $7.071 \cdot 10^{-3}$ ms, although the widening of the damage-band still appears, the branching phenomenon is suppressed. As the rate-dependency of the toughness is further increased through τ_ϵ, the suppression of the branching occurs as well as a shorter crack is observed.

Regarding the crack tip speeds shown in Fig. 9(b), in all cases, the crack appears to be instantly initiated with an initial tip speed that depends upon the rate-dependency of the fracture toughness. As mentioned previously, the strain-rates are the larger at the notch and so is the fracture toughness g_c. This directly influences the initial crack-tip speeds. For small characteristic times τ_ϵ, the cracks accelerate towards a plateau value. Both the acceleration and the plateau values are dependent on τ_ϵ. In the cases where the crack branches, similar values of the plateau $v_c \simeq 640$ m/s are reached before branching. At $\tau_\epsilon = 7.071 \cdot 10^{-3}$ ms, after the plateau, and as no branching occurs, the crack re-accelerates to reach a slightly higher value of $v_c \simeq 680$ m/s and surpasses the value of $0.72c_R$. For larger τ_ϵ, no acceleration of the crack appears; instead, the crack conserves its initial tip-speed which is dependent on τ_ϵ. An increased value of τ_ϵ increases the toughness g_c of the material and hence increases the amount of energy necessary to evolve a crack for the same strain-rates. This directly translates to a smaller value of the phase-field for the same driving force. This in its turn results in a lower possibility of branching.

In Fig. 9(c), the evolution of the toughness at the crack-tip is reported for different characteristic times τ_ϵ. The fracture toughness at the crack-tip is determined as the maximum value of $g_c(\dot{\epsilon})$ (Eq. (20)) in a confined region of size $2 \times l_c$ around the crack-tip. Of course, larger values of g_c are expected for larger τ_ϵ. Observing the cases in which the crack widens without branching ($\tau_\epsilon = 7.071 \cdot 10^{-4}, 10^{-3}$, $2.236 \cdot 10^{-3}$ and $3.162 \cdot 10^{-3}$), the influence of the widening on lowering the strain-rates (Section 3.1) directly impacts the evolution of the toughness: a decline in g_c is first observed as the crack widens and then g_c slightly increases as the crack tightens (Figs. 9(a) and 9(c)). Plus, in the case in which the crack re-accelerates after widening, the fracture toughness g_c appears to increase as the crack re-accelerates, since the strain-rates at the crack-tip increase at the crack tightens which is subsequently transferred to the values of g_c. In the cases where the crack decelerates ($\tau_\epsilon = 3.162 \cdot 10^{-3}$ ms), the toughness drops from an initially higher values to its respective plateau.

To resume, the simulations demonstrate how the strain-rate formulation of the fracture toughness highly influences the dynamic behaviour of fracture. The influence of the strain-rate dependency of the fracture toughness in suppressing the crack-branching and potentially accelerating the crack tip is put forth. The evolution of the strain-rates as the crack widens and their direct impact on the evolution of the fracture toughness are highlighted. The strain-rate dependency of the fracture toughness is shown to play a major role in the dynamic fracture process.

3.4. Damage-rate dependent fracture toughness

To analyse the influence of the damage-rate dependent toughness on the dynamic crack propagation, a purely elastic bulk is considered. The material properties and phase-field parameters are the same as the ones found in Table 1. Simulations are explored for the same imposed vertical displacement $u_0 = 0.0741$ mm. Materials with different damage-rate-dependent toughness (0 — rate-independent toughness$\leq \tau_d \leq 10^{-4}$ ms) are analysed. It is recalled that τ_d corresponds to the amount of the dependency of the toughness to the damage-rate. Only the characteristic times that yielded the most compelling results are exhaustively reported ($\tau_d = 0$, 10^{-6}, $4 \cdot 10^{-6}$, $5 \cdot 10^{-6}$, $2.225 \cdot 10^{-5}$, $2.275 \cdot 10^{-5}$ and $2.288 \cdot 10^{-5}$ ms).

Fig. 10(a) shows the crack path in the fine-mesh region with respect to the characteristic time τ_d. A clear broadening of the damage-band is observed in the materials with the characteristic times $\tau_d = 0$, 10^{-6}, $4 \cdot 10^{-6}$ and $5 \cdot 10^{-6}$ ms. Crack branching occurs in the materials with the characteristic times $\tau_d = 0$, 10^{-6} and $4 \cdot 10^{-6}$ ms. As the characteristic time of the material increases, the rate-dependency of its toughness g_c also increases. This leads to crack widening and branching phenomena to occur after the cracks have travelled longer distances. At τ_d around $5 \cdot 10^{-6}$ ms, although the widening of the damage-band still appears, the branching phenomenon is suppressed. As the rate-dependency of the toughness is further increased through τ_d, in addition to the suppression of the branching and the widening, a shorter crack is observed, even for small variations of τ_d.

Regarding the crack tip speeds shown in Fig. 10(b), in all cases, the crack appears to be instantly initiated at initial tip speeds v_c that depend upon the characteristic time τ_d of the materials. Except for the largest value $\tau_d = 2.288 \cdot 10^{-5}$ ms, the crack accelerates

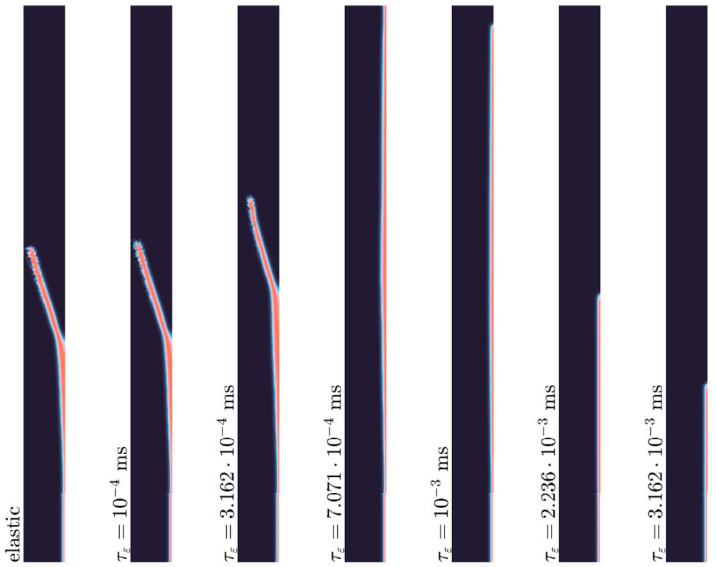

(a) Fracture patterns

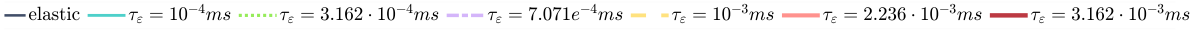

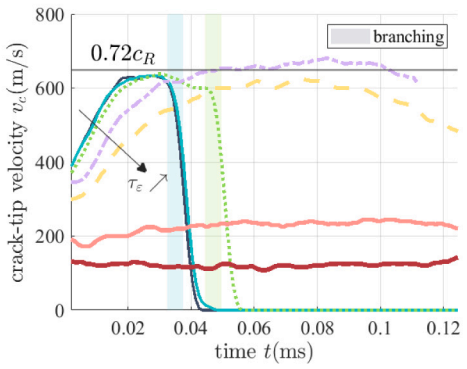

(b) Crack-tip velocities

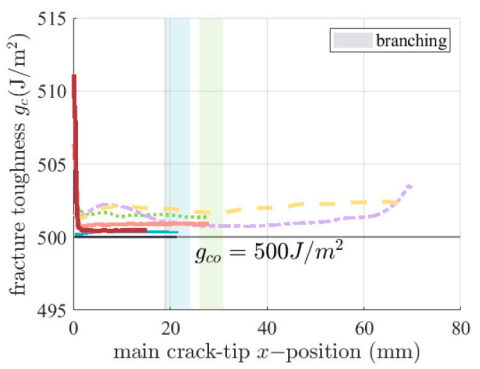

(c) Toughness at the crack-tip

Fig. 9. Elastic materials with strain-rate dependent fracture toughness (τ_ε): uniform displacement strip results at $u_0 = 0.0741$ mm.

towards a plateau value. If the acceleration is dependent on τ_d, even for large τ_d, the plateau v_c remains fairly high at around $v_c = 500$ m/s, unlike in the viscoelastic materials and elastic materials with strain-rate dependent simulations where the plateau value gradually decreases with the characteristic time. For $\tau_d = 2.288 \cdot 10^{-5}$ ms, the crack decelerates from its initial value and oscillates between $0 \leq v_c \leq 10$ m/s. In the cases where the crack-branches, similar values of the plateau $v_c \simeq 640$ m/s are reached before branching. At $\tau_d = 5 \cdot 10^{-6}$ ms, after the plateau, and as no branching occurs, the crack re-accelerates to reach a slightly higher value of $v_c \simeq 660$ m/s and surpasses the value of $0.72c_R$. An increased value of τ_d increases the toughness g_c and hence increases amount of energy necessary to evolve a crack for the same damage-rates, this directly translates to a smaller value of the phase-field for the same driving force, which in its turn results in a lower possibility of the establishment of two spatially separated crack tips around the widened region of the damage-band.

In Fig. 10(c), the evolution of the toughness at the crack-tip is reported for different characteristic times τ_d. The fracture toughness at the crack-tip is determined as the maximum value of $g_c(\dot{d})$ (Eq. (29)) in a confined region of size $2 \times l_c$ around the crack-tip. Of course, larger values of the fracture toughness g_c are expected for larger rate-dependencies τ_d. For each τ_d, the toughness rapidly reaches a plateau. At the case in which the crack re-accelerates after widening, the fracture toughness g_c appears to increase. As the crack re-accelerates, the damage-rates at the crack-tip increase and this increase is subsequently transferred to the values of the toughness g_c. At the larger rate dependency ($\tau_d = 2.225 \cdot 10^{-5}$ and $2.275 \cdot 10^{-5}$ ms) at which the cracks slowly accelerate to reach the plateaus around $v_c = 500$ m/s, the evolution of the toughness g_c at the crack tip is similar. In the case where the crack oscillates

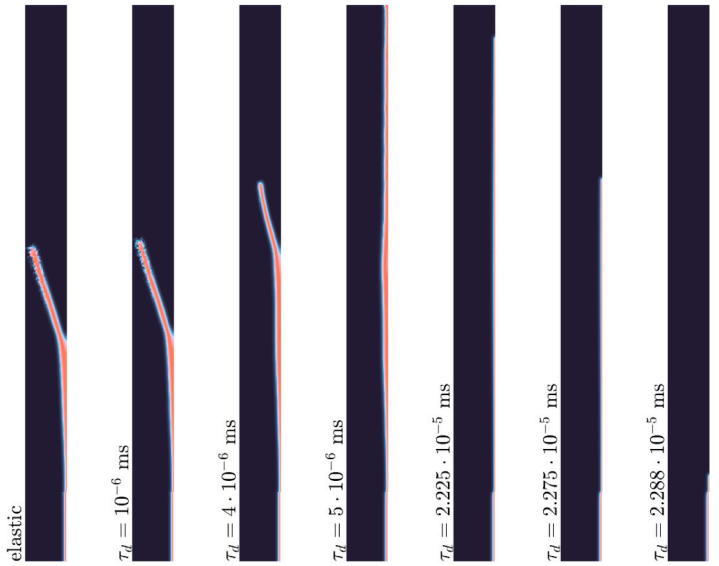

(a) Fracture patterns

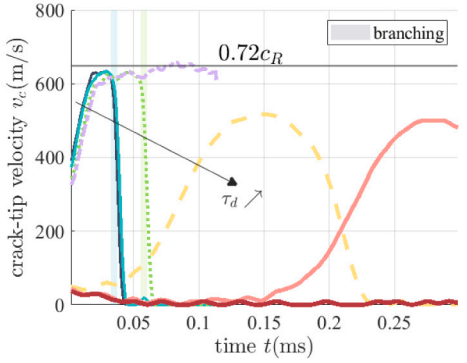

(b) Crack-tip velocities

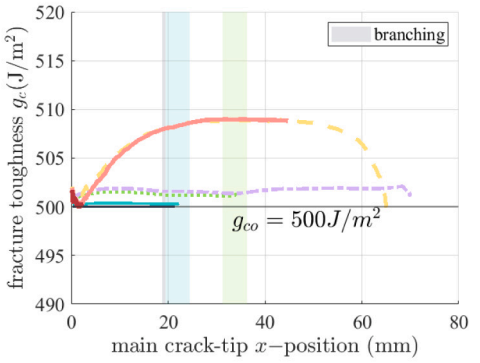

(c) Toughness at the crack-tip

Fig. 10. Elastic materials with damage-rate dependent fracture toughness (τ_d): uniform displacement strip results at $u_0 = 0.0741$ mm.

($\tau_d = 2.288 \cdot 10^{-5}$ ms), the toughness drops from an initial value to its static value, as the crack stops since no more free energy is available for dynamic propagation.

To resume, the simulations demonstrate how the damage-rate formulation of the fracture toughness highly influences the dynamic behaviour of fracture. The influence of the damage-rate dependency of the fracture toughness in suppressing the crack-branching and potentially slightly accelerating the crack tip is put forth. The damage-rate dependency of the fracture toughness is shown to play a major role in the dynamic fracture process.

4. Crack-tip velocity vs. characteristic time

After putting forth the numerical simulation results of the different modelling assumptions for rate-dependent phase-field of fracture, we superpose the obtained limiting tip velocities as a function of the models' characteristic times: τ_v, τ_ϵ or τ_d in Fig. 11.

Basically, at low rate-dependency of the different modelling assumptions, the limiting tip-speed is not impacted until the point where the crack branching is suppressed. Here, the limiting tip speed increases slightly above $v_c = 0.72c_R$. When branching is suppressed, a single crack would propagate straight, and this can actually explain this increase in the crack velocity as compared to the branching cracks case. With an increase in rate-dependency, either the energy dissipated by the material increases, or amount

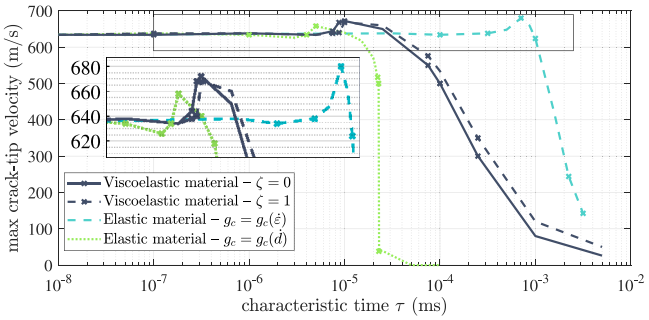

Fig. 11. Influence of the models' characteristic time (τ_v) on the maximum crack-tip speed (imposed vertical displacement $u_0 = 0.0741$ mm).

of energy necessary to evolve a crack increase for the same total available energy. In any case, this leads to the suppression of crack branching and a reduction in the limiting speed, causing the crack to travel a shorter distance.

For the viscoelastic materials, independently of the contribution of the viscous energy in promoting fracture (ζ), and from the purely elastic bulk of the material up to the point where viscous dissipation suppress branching, the limiting speeds are relatively similar.

As higher viscosities are taken into consideration, the assumption regarding the viscous dissipation and its contribution to fracture promotion (i.e., $\zeta = 1$ or $\zeta = 0$) becomes more significant in determining the limiting crack-tip speeds. This is because the dissipated energy, which is attributed to the viscosity of the material, increases, the former being a promoter of fracture through ζ.

In the simulations involving strain-rate dependent toughness, larger characteristic times are needed to affect crack propagation compared to the viscoelastic (and damage-rate dependent formulations). We believe that this difference is due to the quadratic formulation used for the strain-rate dependent toughness, which is different from the linear assumption made for the damage-rate.

For the damage-rate dependent toughness, surprisingly, the drop in the limiting speed as a function the damage-dependency (τ_d) is much steeper. In fact, as seen in the previous section, the plateau reached after an initially accelerating crack is fairly high with the minimum value at around $v_c = 500$ m/s. However a gradual increase of τ_d does not translate to a gradual decrease of the acceleration of the crack or the gradual lowering of the plateau, but it directly translates to a deceleration of the crack speed below $v_c = 100$ m/s.

5. Effective stiffening in rate-dependent materials

After presenting the influence of different modelling assumptions on the rate-dependent fracture, we explore the influence of the stiffening phenomenon usually observed in viscoelastic materials [60] on the fracture behaviour. For instance, it is well known that the behaviour of PMMA is viscoelastic. However, it is possible to model its behaviour by considering a higher elastic stiffness for dynamic analysis as compared to quasi-static simulations [9,73].

In this section we analyse the stiffening of the rate-dependent materials. Further, we look into whether the rate-dependent phase-field models are able to replicate fracture at speeds higher than the expected limitation around $0.75c_R$ found in similar configurations [51].

In order to achieve this goal, we will take into account the three modelling assumptions, which involve simulating uniform displacement strips using four arbitrary materials that exhibit high rate-dependencies. Higher pre-strain are considered with imposed displacement $0.0741 \leq u_0 \leq 0.1995$ mm. As seen in Ref. [5], larger pre-strains directly affect the initial crack-tip velocity, its acceleration, its plateau and the possible branching phenomena.

The phase-field parameters and material properties are similar to the ones found in Table 1. The rate-dependent parameters for the different materials are as follow:

1. Viscoelastic material — $\tau_v = 5 \cdot 10^{-3}$ ms with $\zeta = 0$
2. Viscoelastic material — $\tau_v = 5 \cdot 10^{-3}$ ms with $\zeta = 1$
3. Elastic material with strain-rate dependent fracture toughness — $\tau_\varepsilon = 10^{-2}$ ms
4. Elastic material with damage-rate dependent fracture toughness — $\tau_d = 5 \cdot 10^{-5}$ ms

As seen in the previous sections, higher rate-dependencies directly affect the dynamic fracture behaviour. The high rate-dependencies herein considered ensure the suppression of branching even for high pre-strains. Hence, a single crack tip can be followed throughout the fracture process.

Only the maximum crack-tip velocity for each simulation is noted. The evolution of the maximum tip speed as a function of the loadings u_0 is plotted in Fig. 12 for the different materials. At a loading of $u_0 = 0.0741$ mm, the cracks slightly advances at a speed lower than 50 m/s. As the pre-strain is increased, the maximum obtained crack-tip speed increases.

For both viscoelastic models, the crack-speeds are indeed higher than $c_R = 900$ m/s (computed from the material properties in Table 1). In the case where $\zeta = 1$ (the dissipated viscous energy promotes fracture), it is clear how this supplementary driving force

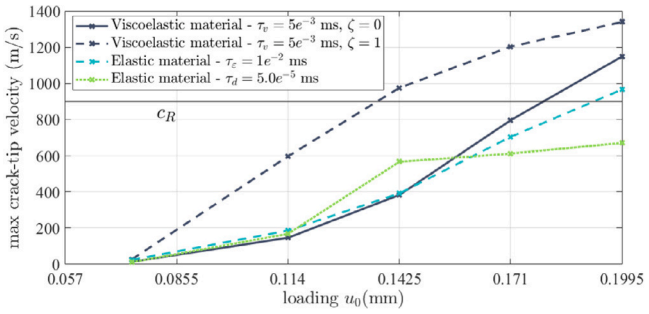

Fig. 12. Maximum crack-tip velocities at multiple loadings.

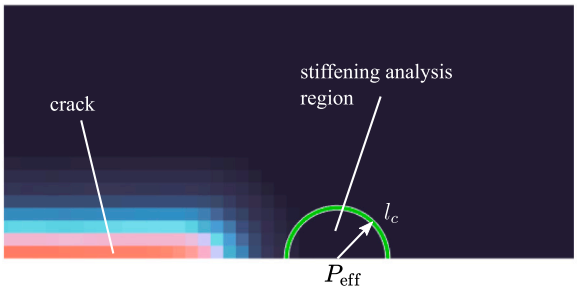

Fig. 13. Stiffening analysis at the crack-tip in rate-dependent materials.

is reflected on the limiting speed that is between 120% and 300% higher than the speed of the crack in the case where $\zeta = 0$. For the strain-rate-dependent toughness, it is observed that the crack-tip reaches a maximum speed $v_c = 966$ m/s $\geq c_R = 900$ m/s at the larger considered pre-strain ($u_0 = 0.1995$ mm). For the damage-rate-dependent toughness, the crack speed is limited by the Rayleigh wave-speed $c_R = 900$ m/s.

How can one explain the crack-tip velocities that exceed the Rayleigh wave speed ? We believe that a stiffening phenomenon in the crack-tip region occurs and is responsible of these faster-running cracks. This idea was previously explored in elastomers [10,14]. In fact, as the material becomes stiffer, the speed of the Rayleigh waves in the stiffened region becomes higher. And a higher Rayleigh wave speed allows faster-running cracks [74].

To further elaborate on this idea, we investigate the apparent stiffness of the material in a confined region in front of the crack. At the crack-tip (Fig. 13), the effective elastic moduli are computed from the stress–strain couples obtained from damage the phase-field simulations following the method proposed in Ref. [39]. In fact, the stiffness is analysed at a single data point (P_{eff}) at a distance l_c in front of the crack, where we compute the average stress and strain tensors in a confined region of size l_c centred at P_{eff}.

The obtained strain and stress couples provide an evaluation of the nine components of the effective stiffness tensor representative of the effective elastic behaviour at the crack tip (more specifically at P_{eff}). From the overall stiffness tensor, and by assuming plane-strain conditions and isotropic elasticity, effective Young's modulus (E_{eff}) and Poisson's ratio (ν_{eff}) can be computed.

The effective Young's modulus and Poisson's ratio at the crack-tip of the two viscoelastic materials are reported in Figs. 14 and 15 (for $\zeta = 0$ and $\zeta = 1$ respectively). In both cases, it is clear how the viscous effects at the crack tip enable the stiffening of the material. The effective Young's modulus at the crack-tip ranges from the static value of 3 GPa to about 6.5 GPa at the highest pre-strains. We mention that the values herein found are reasonably in accordance with mechanical properties identified for PMMA at high strain rates in Ref. [60]. Seghir et al. [60] find the static value of the quasi-static reference material properties for PMMA to be $E = 2.9 \pm 0.1$ GPa, and at high strain rates, the modulus is found to approaches 6 GPa.

The effective Young's modulus and Poisson's ratio at the crack-tip (E_{eff} and ν_{eff} respectively) of the elastic material, which fracture toughness is strain-rate dependent, are reported in Fig. 16. Indeed, a viscous-like stiffening in front of the crack tip is observed. The effective Young's modulus at the crack-tip ranges from the static value of 3 GPa to about 4 GPa at the highest pre-strains. This viscous-like stiffening is actually the fruit of the additional term in the stress that comes from the strain-rate dependent toughness, see Eq. (26) in . Although the characteristic time $\tau_\varepsilon = 10^{-2}$ ms of this material is larger than the characteristic time of the considered viscoelastic materials $\tau_v = 5 \cdot 10^{-3}$ ms, the stiffening at the crack-tip is much less prominent. This is easily explained by the fact that the strain-rate dependency of the toughness yields an additional stress term that only appears in the damaged region and that is absent in the intact region. In viscoelastic materials, the viscous stresses are present both in the bulk and in the damaged region of the material.

The effective Young modulus and Poisson ratio at the crack-tip (E_{eff} and ν_{eff} respectively) of the elastic material which fracture toughness is damage-rate dependent are reported in Fig. 17; as expected no hardening at the crack-tip occurs and the limiting speed is indeed $c_R = 900$ m/s.

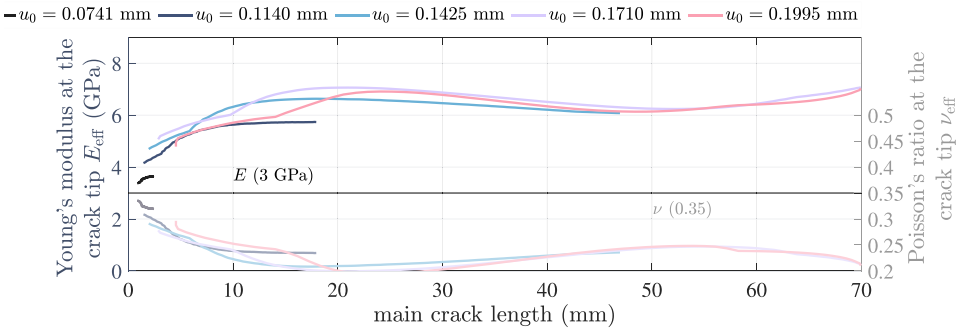

Fig. 14. Effective stiffening at the crack-tip in the viscoelastic material with $\zeta = 0$.

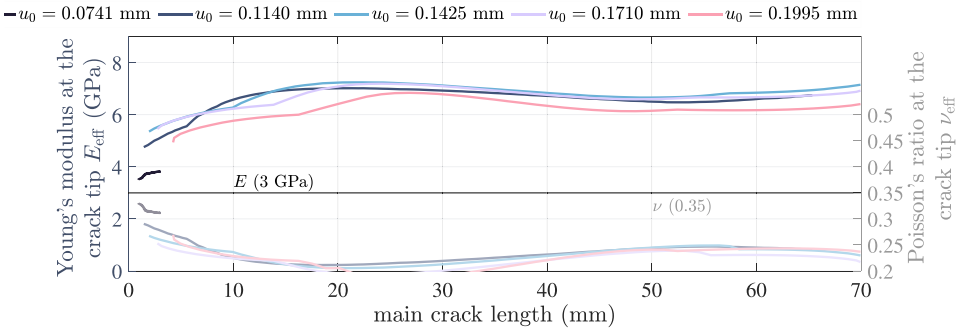

Fig. 15. Effective stiffening at the crack-tip in the viscoelastic material with $\zeta = 1$.

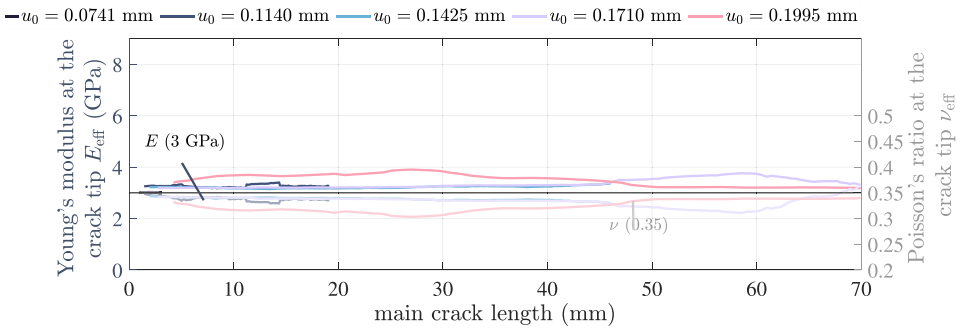

Fig. 16. Effective stiffening at the crack-tip in the material with strain-rate dependent toughness.

The highest values of the Rayleigh wave-speeds at the crack-tip (the Rayleigh wave-speeds being computed following Freund's Eq. (35) considering the effective elastic moduli E_{eff} and ν_{eff} from Figs. 14, 15, 16 and 17), are reported in Table 2 for the four materials and at different pre-strain values.

Indeed, in all cases, the reported speeds of Rayleigh waves at the crack-tip speeds are always higher than the crack-tip speeds recorded in the simulations. In fact, the literature predicts that the flow of energy into a crack-tip falls to zero when the crack runs at the Rayleigh velocity c_R [74,75]. This limits the crack-tip velocity to the Rayleigh wave speed c_R. Plus, the emergence of stiffening phenomena in the crack-tip region in rate-dependent materials increases the velocities of the elastic waves locally. The particular increase in the speed of the Rayleigh waves makes it that the flow of energy to the crack is no longer null, enabling thus the faster-running cracks.

6. Conclusion

This paper revisits the advancements on the rate-dependent phase-field models for fracture and suggests a novel damage-rate dependent formulation for the fracture toughness. By means of a numerical study on a uniform displacement strip benchmark, the formulations and modelling assumptions are contrasted and the corresponding limiting crack speeds are discussed.

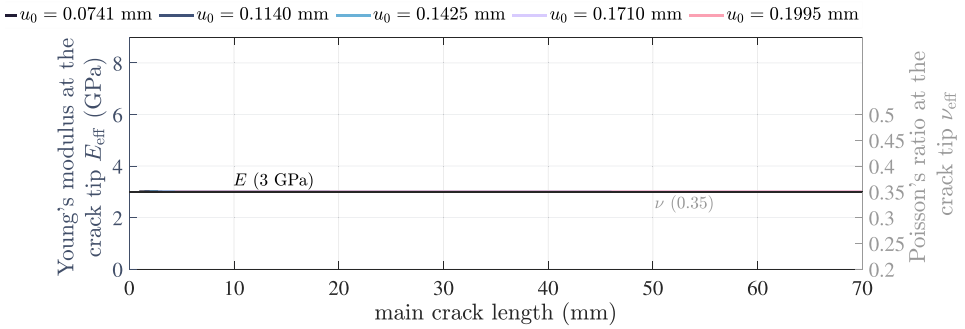

Fig. 17. No stiffening at the crack-tip in the material with damage-rate dependent toughness.

Table 2
Maximum effective Rayleigh wave speed c_R in front of the crack-tip in the different rate-dependent materials under different pre-strains.

Maximum c_R at the crack-tip					
Rate dependency	pre-strain u_0 (mm)				
	0.0741	0.114	0.1425	0.171	0.1995
Viscoelastic material — $\tau_v = 5 \cdot 10^{-3}$ ms, $\zeta = 0$	998 m/s	1277 m/s	1380 m/s	1425 m/s	1422 m/s
Viscoelastic material — $\tau_v = 5 \cdot 10^{-3}$ ms, $\zeta = 1$	1024 m/s	1419 m/s	1444 m/s	1443 m/s	1410 m/s
Strain-rate dependent toughness — $\tau_\epsilon = 10^{-2}$ ms	903 m/s	962 m/s	957 m/s	1016 m/s	1036 m/s
Damage-rate dependent toughness — $\tau_d = 5 \cdot 10^{-5}$ ms	900 m/s	900 m/s	900 m/s	900 m/s	900 m/s

The first formulation [35,36] is characterised by the addition to the pseudo-energy functional of the phase-field problem (free energy and fracture dissipation) a contribution which is related to the viscous dissipation. The viscous dissipation is assumed to promote fracture through a parameter ζ. The parameter ζ can take any value between $\zeta = 0$ (viscous dissipation does not promote fracture) and $\zeta = 1$ (the entirety of the heat produced by the viscous dissipation promotes fracture). The model is based on experimental evidence that shows how the resistance to fracture of many rate-dependent materials decreases as the temperature increases, from one side, and how the viscoelastic dissipation leads to a raise in the temperature of the material from the other.

The second model [46] is characterised by the introduction of a strain-rate dependent toughness $g_c(\dot{\epsilon})$. It is based on experimental evidence that indicates a strong relationship between the rate of strains and the material's resistance against fracture. Alternatively, in the same spirit, we suggested a damage-rate dependent toughness formulation enabling an upper limit on the rate-dependent toughness g_c.

Simulation quantitatively evidence the influence of rate-dependency on the dynamic crack behaviour:

1. Crack branching observed in rate-dependent simulation at a fixed pre-strain can be suppressed with the different modelling assumptions of rate dependency.
2. With the increase of the rate-dependency, and as the branching phenomenon persists, the limiting speeds are unsurprisingly similar for the different models.
3. As the crack branching is omitted, cracks may advance at higher tip speeds, dependently on the rate-dependencies
4. A gradual increase in the rate-dependencies of the viscoelastic materials and materials with strain-rate-dependent toughness gradually modify the dynamic crack behaviour.
5. Even a gradual increase in the damage-rate-dependency of the toughness can translate to abrupt changes in the behaviour of the cracks.

Additionally, we explained the increase of limiting velocity with the local stiffening of the materials. Indeed, depending on the specific choice of parameters, our simulations show crack-tip speeds that exceed c_R in viscoelastic materials (whether the viscous dissipation is assumed to promote fracture or not) and in elastic materials with strain-rate-dependent toughness: these high speeds are attributed to the viscoelastic and viscoelastic-like stiffening quantified at the front of the cracks. In fact, the stiffening phenomenon translates to faster-running surface-waves which in its turn enables faster running cracks. It is noted that the crack-tip speeds are consistently lower than the effective surface-wave speeds, i.e., the Rayleigh wave speeds in the stiffened region at the crack tip.

Future work will focus on the comparison of those model predictions and experimental data to further assess the modelling choices. Besides, we believe that combining the viscoelastic model with damage-rate dependency of the toughness, and accurately calibrating the damage-rate dependence τ_d for the actual experiments, may enable the reproduction of intermittent cracking behaviour observed in PMMA [76].

CRediT authorship contribution statement

Elie Eid: Writing – review & editing, Writing – original draft, Validation, Methodology, Investigation, Formal analysis, Conceptualization. **Anthony Gravouil:** Writing – review & editing, Validation, Supervision, Formal analysis, Conceptualization. **Gergely Molnár:** Writing – review & editing, Validation, Supervision, Resources, Methodology, Funding acquisition, Formal analysis, Conceptualization.

Declaration of competing interest

The authors declare that they have no known competing financial interests or personal relationships that could have appeared to influence the work reported in this paper.

Data availability

Data will be made available on request.

Acknowledgements

This work was supported by the French Research National Agency program e-WARNINGS (ANR-19-CE42-0012–04).

Appendix. Constitutive modelling of the viscoelastic bulk

This appendix overviews the full constitutive modelling of the intact viscoelastic bulk following the work of Luo et al. [62]. As mentioned in Section 2.1, a Kelvin–Voigt approach is employed to analyse the spheric portion of the stress–strain behaviour (Fig. 2(a)), and a Maxwell-like model is utilised for the deviatoric part of the stress–strain behaviour (Fig. 2(b)).

The hydrostatic stress–strain relation at time t can then be expressed as:

$$\bar{\sigma}^{hyd}(t) = K_d[\epsilon^{hyd}(t) + \tau_{vd}\dot{\epsilon}^{hyd}(t)] \tag{36}$$

where $\tau_{vd} = \eta_d / K_d$ is the bulk relaxation time, η_d is the bulk viscosity and K_d is the bulk modulus. The superscript hyd correspond the hydrostatic stresses $\bar{\sigma}$ and strains ϵ.

$$\bar{\sigma}^{dev}(t) + \tau_{vs}\dot{\bar{\sigma}}(t) = K_s[\epsilon^{dev}(t) + 2\tau_{vs}\dot{\epsilon}^{dev}(t)] \tag{37}$$

where $\tau_{vs} = \eta_s / K_s$ is the shear relaxation time, η_s is the shear viscosity and K_s is the shear modulus. The superscript dev corresponds to the deviatoric stresses and strains. To obtain the overall stress–strain expressions, the time-domain expressions Eqs. (36) and (37) have to be solved. Here, the stresses functions of the strains are directly exposed, the detailed derivations can be found in Ref. [62]:

$$\bar{\sigma}(t) = \frac{E}{1-2\nu}[\epsilon^{hyd}(t) + \tau_{vd}\dot{\epsilon}^{hyd}(t)] + \frac{E}{1+\nu}\epsilon^{dev}(t) + h(t) \tag{38}$$

where $h(t)$ is to be defined by a recurrence relation following:

$$h(t) = \exp\left(-\frac{t-t_n}{\tau_{vs}}\right)h(t_n) + \frac{E}{1+\nu}\int_{t_n}^{t}\exp\left(-\frac{t-t'}{\tau_{vs}}\right)\dot{\epsilon}^{dev}(t)dt' \tag{39}$$

where E is Young's Modulus and ν Poisson's ratio and t_n is any moment before t. In addition to the full separation of the deviatoric and hydrostatic parts, this formulation displays an intriguing structure: a complete split between the elastic properties and the viscous components, so one can write :

$$\bar{\sigma}_e^{hyd}(t) = \frac{E}{1-2\nu}\epsilon^{hyd}(t) \tag{40a}$$

$$\bar{\sigma}_v^{hyd}(t) = \frac{E}{1-2\nu}\tau_{vd}\dot{\epsilon}^{hyd}(t) \tag{40b}$$

$$\bar{\sigma}_e^{dev}(t) = \frac{E}{1+\nu}\epsilon^{dev}(t) \tag{40c}$$

$$\bar{\sigma}_v^{dev}(t) = \exp\left(-\frac{t-t_n}{\tau_{vs}}\right)h(t_n) + \frac{E}{1+\nu}\int_{t_n}^{t}\exp\left(-\frac{t-t'}{\tau_{vs}}\right)\dot{\epsilon}^{dev}(t)dt' \tag{40d}$$

The subscripts e and v correspond to the elastic/viscous parts of the strains and stresses.

References

[1] D'Amico F, Carbone G, Foglia M, Galietti U. Moving cracks in viscoelastic materials: Temperature and energy-release-rate measurements. Eng Fract Mech 2013;98:315–25. http://dx.doi.org/10.1016/j.engfracmech.2012.10.026, URL https://linkinghub.elsevier.com/retrieve/pii/S0013794412004353.

[2] Ramulu M, Kobayashi AS. Dynamic crack curving—A photoelastic evaluation. Exp Mech 1983;23(1):1–9. http://dx.doi.org/10.1007/BF02328674, URL http://link.springer.com/10.1007/BF02328674.

[3] Streit R, Finnie I. An experimental investigation of crack-path directional stability: A photoelastic and experimental study on the effect of crack-tip stress biaxiality with respect to directional stability and fracture toughness of Mode I crack extension. Exp Mech 1980;20(1):17–23. http://dx.doi.org/10.1007/BF02324422, URL http://link.springer.com/10.1007/BF02324422.

[4] Fineberg J, Gross SP, Marder M, Swinney HL. Instability in dynamic fracture. Phys. Rev. Lett. 1991;67(4):457–60. http://dx.doi.org/10.1103/PhysRevLett.67.457, https://link.aps.org/doi/10.1103/PhysRevLett.67.457.

[5] Bleyer J, Roux-Langlois C, Molinari J-F. Dynamic crack propagation with a variational phase-field model: limiting speed, crack branching and velocity-toughening mechanisms. Int J Fract 2017;204(1):79–100. http://dx.doi.org/10.1007/s10704-016-0163-1, URL http://link.springer.com/10.1007/s10704-016-0163-1.

[6] Liu G, Li Q, Msekh MA, Zuo Z. Abaqus implementation of monolithic and staggered schemes for quasi-static and dynamic fracture phase-field model. Comput Mater Sci 2016;121:35–47. http://dx.doi.org/10.1016/j.commatsci.2016.04.009, URL https://linkinghub.elsevier.com/retrieve/pii/S0927025616301550.

[7] Pham KH, Ravi-Chandar K, Landis CM. Experimental validation of a phase-field model for fracture. Int J Fract 2017;205(1):83–101. http://dx.doi.org/10.1007/s10704-017-0185-3, URL http://link.springer.com/10.1007/s10704-017-0185-3.

[8] Ren H, Zhuang X, Anitescu C, Rabczuk T. An explicit phase field method for brittle dynamic fracture. Comput Struct 2019;217:45–56. http://dx.doi.org/10.1016/j.compstruc.2019.03.005, URL https://linkinghub.elsevier.com/retrieve/pii/S0045794918311003.

[9] Eid E, Seghir R, Réthoré J. Crack branching at low tip speeds: spilling the T. Journal of Theoretical, Computational and Applied Mechanics 2023. http://dx.doi.org/10.46298/jtcam.10172, http://jtcam.episciences.org/12218.

[10] Corre T, Coret M, Verron E, Leblé B, Le Lay F. Experimental full field analysis for dynamic fracture of elastomer membranes. Int J Fract 2020;224:83–100.

[11] Morishita Y, Tsunoda K, Urayama K. Velocity transition in the crack growth dynamics of filled elastomers: Contributions of nonlinear viscoelasticity. Phys Rev E 2016;93:043001. http://dx.doi.org/10.1103/PhysRevE.93.043001, URL https://link.aps.org/doi/10.1103/PhysRevE.93.043001.

[12] Gent AN, Marteny P. The effect of strain upon the velocity of sound and the velocity of free retraction for natural rubber. J Appl Phys 1982-09;53(9):6069–75. http://dx.doi.org/10.1063/1.331558, _eprint: https://pubs.aip.org/aip/jap/article-pdf/53/9/6069/7978356/6069_1_online.pdf.

[13] Stevenson A, Thomas AG. On the bursting of a balloon. J Phys D: Appl Phys 1979;12(12):2101. http://dx.doi.org/10.1088/0022-3727/12/12/012.

[14] Kamasamudram V, Coret M, Moës N. The role played by viscoelasticity in the bulk material during the propagation of a dynamic crack in elastomers. Int J Fract 2021;231:43–58.

[15] Knauss WG. A review of fracture in viscoelastic materials. Int J Fract 2015-11-01;196(1):99–146. http://dx.doi.org/10.1007/s10704-015-0058-6.

[16] Thouless MD, Hsueh C-H, Evans AG. A damage model of creep crack growth in polycrystals. Acta Metall 1983;31:1675–87, URL https://api.semanticscholar.org/CorpusID:136746414.

[17] Schapery RA. Correspondence principles and a generalizedJ integral for large deformation and fracture analysis of viscoelastic media. Int J Fract 1984-07-01;25(3):195–223. http://dx.doi.org/10.1007/BF01140837.

[18] Kroon M. Steady-state crack growth in rubber-like solids. Int J Fract 2011-05-01;169(1):49–60. http://dx.doi.org/10.1007/s10704-010-9583-5.

[19] Zhang H, Rong G, Li L. Numerical study on deformations in a cracked viscoelastic body with the extended finite element method. Eng Anal Bound Elem 2010;34(6):619–24. http://dx.doi.org/10.1016/j.enganabound.2010.02.001, URL https://www.sciencedirect.com/science/article/pii/S0955799710000184.

[20] Moes N, Dolbow J, Belytschko T. A finite element method for crack growth without remeshing. 1999, p. 20.

[21] Bažant ZP, Li Y-N. Cohesive crack with rate-dependent opening and viscoelasticity: I. mathematical model and scaling. Int J Fract 1997;86:247–65, URL https://api.semanticscholar.org/CorpusID:14511346.

[22] Hillerborg A, Modéer M, Petersson P-E. Analysis of crack formation and crack growth in concrete by means of fracture mechanics and finite elements. Cem Concr Res 1976;6(6):773–81. http://dx.doi.org/10.1016/0008-8846(76)90007-7, URL https://www.sciencedirect.com/science/article/pii/0008884676900077.

[23] Yoon C, Allen DH. Damage dependent constitutive behavior and energy release rate for a cohesive zone in a thermoviscoelastic solid. Int J Fract 1999;96(1):55–74. http://dx.doi.org/10.1023/A:1018601004565.

[24] Kachanov L. Introduction to continuum damage mechanics, vol. 10. Springer Science & Business Media; 1986.

[25] Wolff C, Richart N, Molinari J-F. A non-local continuum damage approach to model dynamic crack branching. Int J Numer Methods Eng 2015;101(12):933–49. http://dx.doi.org/10.1002/nme.4837, URL https://hal.univ-lorraine.fr/hal-01417917.

[26] Abdullah T, Kirane K. Continuum damage modeling of dynamic crack velocity, branching, and energy dissipation in brittle materials. Int J Fract 2021;229:15–37, URL https://api.semanticscholar.org/CorpusID:233330453.

[27] Bourdin B, Francfort G, Marigo J-J. Numerical experiments in revisited brittle fracture. J Mech Phys Solids 2000;48(4):797–826. http://dx.doi.org/10.1016/S0022-5096(99)00028-9, URL https://linkinghub.elsevier.com/retrieve/pii/S0022509699000289.

[28] Francfort G, Marigo J-J. Revisiting brittle fracture as an energy minimization problem. J Mech Phys Solids 1998;46(8):1319–42. http://dx.doi.org/10.1016/S0022-5096(98)00034-9, URL https://linkinghub.elsevier.com/retrieve/pii/S0022509698000349.

[29] Griffith AA. VI. The phenomena of rupture and flow in solids. Phil Trans R Soc Lond Ser A 1921;221(582–593):163–98, Publisher: The royal society London.

[30] Borden MJ, Hughes TJ, Landis CM, Anvari A, Lee IJ. A phase-field formulation for fracture in ductile materials: Finite deformation balance law derivation, plastic degradation, and stress triaxiality effects. Comput Methods Appl Mech Engrg 2016;312:130–66. http://dx.doi.org/10.1016/j.cma.2016.09.005, Phase Field Approaches to Fracture, URL https://www.sciencedirect.com/science/article/pii/S0045782516311069.

[31] Liu G, Li Q, Msekh MA, Zuo Z. Abaqus implementation of monolithic and staggered schemes for quasi-static and dynamic fracture phase-field model. Comput Mater Sci 2016;121:35–47. http://dx.doi.org/10.1016/j.commatsci.2016.04.009, URL https://www.sciencedirect.com/science/article/pii/S0927025616301550.

[32] Molnár G, Gravouil A, Seghir R, Réthoré J. An open-source Abaqus implementation of the phase-field method to study the effect of plasticity on the instantaneous fracture toughness in dynamic crack propagation. Comput Methods Appl Mech Engrg 2020;365:113004. http://dx.doi.org/10.1016/j.cma.2020.113004, URL https://linkinghub.elsevier.com/retrieve/pii/S0045782520301882.

[33] Miehe C, Hofacker M, Schänzel L-M, Aldakheel F. Phase field modeling of fracture in multi-physics problems. Part II. coupled brittle-to-ductile failure criteria and crack propagation in thermo-elastic–plastic solids. Comput Methods Appl Mech Engrg 2015;294:486–522.

[34] Schänzel L-M. Phase field modeling of fracture in rubbery and glassy polymers at finite thermo-viscoelastic deformations. 2015.

[35] Shen R, Waisman H, Guo L. Fracture of viscoelastic solids modeled with a modified phase field method. Comput Methods Appl Mech Engrg 2019;346:862–90. http://dx.doi.org/10.1016/j.cma.2018.09.018, URL https://linkinghub.elsevier.com/retrieve/pii/S0045782518304699.

[36] Dammaß F, Ambati M, Kästner M. A unified phase-field model of fracture in viscoelastic materials. Contin Mech Thermodyn 2021;33(4):1907–29. http://dx.doi.org/10.1007/s00161-021-01013-3, URL https://link.springer.com/10.1007/s00161-021-01013-3.

[37] Hai L, Li J. A rate-dependent phase-field framework for the dynamic failure of quasi-brittle materials. Eng Fract Mech 2021;252:107847. http://dx.doi.org/10.1016/j.engfracmech.2021.107847, URL https://www.sciencedirect.com/science/article/pii/S001379442100285X.

[38] Shanthraj P, Svendsen B, Sharma L, Roters F, Raabe D. Elasto-viscoplastic phase field modelling of anisotropic cleavage fracture. J Mech Phys Solids 2017;99:19–34.

[39] Eid E, Seghir R, Réthoré J. Multiscale analysis of brittle failure in heterogeneous materials. J Mech Phys Solids 2021;146:104204. http://dx.doi.org/10.1016/j.jmps.2020.104204, URL https://linkinghub.elsevier.com/retrieve/pii/S0022509620304257.

[40] Chen W, Tan VBC, Zeng X, Li P. FE2 methodology for discrete cohesive crack propagation in heterogenous materials. Eng Fract Mech 2022;269:108537.

[41] Tsunoda K, Busfield J, Davies C, Thomas A. Effect of materials variables on the tear behaviour of a non-crystallising elastomer. J Mater Sci 2000;35:5187–98.

[42] Carbone G, Persson B. Crack motion in viscoelastic solids: the role of the flash temperature. Eur Phys J E 2005;17:261–81.

[43] Loew PJ, Peters B, Beex LA. Rate-dependent phase-field damage modeling of rubber and its experimental parameter identification. J Mech Phys Solids 2019;127:266–94. http://dx.doi.org/10.1016/j.jmps.2019.03.022, URL https://www.sciencedirect.com/science/article/pii/S0022509618310433.

[44] Kanninen MF, McEvily A, Popelar CH. Advanced fracture mechanics. The American Society of Mechanical Engineers (ASME); 1986.

[45] Dally J, Fourney W, Irwin G. On the uniqueness of the stress intensity factor—crack velocity relationship. Dyn Fract 1985;33–42.

[46] Yin B, Steinke C, Kaliske M. Formulation and implementation of strain rate-dependent fracture toughness in context of the phase-field method. Internat J Numer Methods Engrg 2020;121(2):233–55.

[47] Gamonpilas C, Charalambides M, Williams J. Determination of large deformation and fracture behaviour of starch gels from conventional and wire cutting experiments. J Mater Sci 2009;44:4976–86.

[48] Dammaß F, Kalina KA, Ambati M, Kästner M. Phase-field modelling and analysis of rate-dependent fracture phenomena at finite deformation. Comput Mech 2023-04-18. http://dx.doi.org/10.1007/s00466-023-02310-1.

[49] Nilsson F. Crack propagation experiments on strip specimens. Eng Fract Mech 1974;6(2):397–403.

[50] Freund LB. Dynamic fracture mechanics. Cambridge University Press; 1998.

[51] Zhou F. Study on the macroscopic behavior and the microscopic process of dynamic crack propagation [Ph.D. thesis], Tokyo: The University of Tokyo; 1996.

[52] Borgnakke C, Sonntag RE. Fundamentals of thermodynamics. John Wiley & Sons; 2022.

[53] Halphen B, Son Nguyen Q. Sur les matériaux standard généralisés. J Méc 1975;14(1):39–63, URL https://hal.science/hal-03600755.

[54] Amor H, Marigo J-J, Maurini C. Regularized formulation of the variational brittle fracture with unilateral contact: Numerical experiments. J Mech Phys Solids 2009;57(8):1209–29. http://dx.doi.org/10.1016/j.jmps.2009.04.011, URL https://linkinghub.elsevier.com/retrieve/pii/S0022509609000659.

[55] Miehe C, Hofacker M, Welschinger F. A phase field model for rate-independent crack propagation: Robust algorithmic implementation based on operator splits. Comput Methods Appl Mech Engrg 2010;199(45–48):2765–78. http://dx.doi.org/10.1016/j.cma.2010.04.011, URL https://linkinghub.elsevier.com/retrieve/pii/S0045782510001283.

[56] Molnár G, Doitrand A, Jaccon A, Prabel B, Gravouil A. Thermodynamically consistent linear-gradient damage model in Abaqus. Eng Fract Mech 2022;266:108390.

[57] Lemaître J, Chaboche J-L. Mechanics of solid materials. Cambridge: Cambridge University Press; 1990.

[58] Mehrmashhadi J, Wang L, Bobaru F. Uncovering the dynamic fracture behavior of PMMA with peridynamics: The importance of softening at the crack tip. Eng Fract Mech 2019;219:106617. http://dx.doi.org/10.1016/j.engfracmech.2019.106617, URL https://www.sciencedirect.com/science/article/pii/S0013794419306484.

[59] Capodagli J, Lakes R. Isothermal viscoelastic properties of PMMA and LDPE over 11 decades of frequency and time: a test of time–temperature superposition. Rheol Acta 2008;47(7):777–86. http://dx.doi.org/10.1007/s00397-008-0287-y.

[60] Seghir R, Pierron F. A novel image-based ultrasonic test to map material mechanical properties at high strain-rates. Exp Mech 2018;58(2):183–206. http://dx.doi.org/10.1007/s11340-017-0329-4, URL http://link.springer.com/10.1007/s11340-017-0329-4.

[61] Tschoegl NW. The phenomenological theory of linear viscoelastic behavior. Berlin, Heidelberg: Springer Berlin Heidelberg; 1989, http://dx.doi.org/10.1007/978-3-642-73602-5, URL http://link.springer.com/10.1007/978-3-642-73602-5.

[62] Luo H, Gravouil A, Giordano VM, Schirmacher W, Tanguy A. Continuum constitutive laws to describe acoustic attenuation in glasses. Phys Rev E 2020;102(3):033003. http://dx.doi.org/10.1103/PhysRevE.102.033003, URL https://link.aps.org/doi/10.1103/PhysRevE.102.033003.

[63] Kaliske M, Rothert H. Formulation and implementation of three-dimensional viscoelasticity at small and finite strains. Comput Mech 1997;19(3):228–39. http://dx.doi.org/10.1007/s004660050171, URL http://link.springer.com/10.1007/s004660050171.

[64] Fineberg J, Gross SP, Marder M, Swinney HL. Instability in the propagation of fast cracks. Phys Rev B 1992;45(10):5146.

[65] Bischoff P, Perry S. Compressive behaviour of concrete at high strain rates. Mater Struct 1991;24:425–50.

[66] Sharon E, Gross SP, Fineberg J. Energy dissipation in dynamic fracture. Phys Rev Lett 1996;76(12):2117.

[67] Bleyer J, Roux-Langlois C, Molinari J-F. Dynamic crack propagation with a variational phase-field model: limiting speed, crack branching and velocity-toughening mechanisms. Int J Fract 2017;204(1):79–100. http://dx.doi.org/10.1007/s10704-016-0163-1, URL http://link.springer.com/10.1007/s10704-016-0163-1.

[68] Özenç K. Approaches to model failure of materials by configurational mechanics: theory and numerics [Ph.D. thesis], Technische Universität Dresden; 2016.

[69] Molnár G, Gravouil A. 2D and 3D abaqus implementation of a robust staggered phase-field solution for modeling brittle fracture. Finite Elem Anal Des 2017;130:27–38.

[70] Doitrand A, Molnár G, Leguillon D, Martin E, Carrère N. Dynamic crack initiation assessment with the coupled criterion. Eur J Mech A Solids 2022;93:104483.

[71] Yoffe EH. LXXV. The moving Griffith crack. null 1951;42(330):739–50. http://dx.doi.org/10.1080/14786445108561302, Publisher: Taylor & Francis.

[72] Hilber HM, Hughes TJ, Taylor RL. Improved numerical dissipation for time integration algorithms in structural dynamics. Earthq Eng Struct Dyn 1977;5(3):283–92.

[73] Grégoire D, Maigre H, Rethore J, Combescure A. Dynamic crack propagation under mixed-mode loading–comparison between experiments and X-FEM simulations. Int J Solids Struct 2007;44(20):6517–34.

[74] Atkinson C, Eshelby J. The flow of energy into the tip of a moving crack. Int J Fract Mech 1968;4:3–8.

[75] Broberg KB. How fast can a crack go? Mater Sci 1996;32(1):80–6. http://dx.doi.org/10.1007/BF02538928, URL http://link.springer.com/10.1007/BF02538928.

[76] Heinzmann R, Seghir R, Alam S-Y, Réthoré J. Experimental investigation of the alternate recurrence of quasi-static and dynamic crack propagation in PMMA. 2023, http://dx.doi.org/10.21203/rs.3.rs-2498972/v1 [submitted for publication].